A Vulnerability of a Subset of Colon Cancers with Potential Clinical Utility

A vulnerability of a subset of colon cancers with potential clinical utility

Loredana Vecchione[1#], Valentina Gambino[1#], Jonne Raaijmakers[2], Andreas Schlicker[1], Arianna Fumagalli[3], Mariangela Russo[4,5,6], Alberto Villanueva[7], Evelyne Beerling[3], Alice Bartolini[5], David G. Mollevi[7], Nizar El-Murr[8], Marielle Chiron[8], Loreley Calvet[8], Céline Nicolazzi[8], Cécile Combeau[8], Christophe Henry[8], Iris M. Simon[9], Sun Tian[9], Sjors in 't Veld[9], Giovanni D'ario[10], Sara Mainardi[1] , Roderick L Beijersbergen[1], Cor Lieftink[1], Sabine Linn[11], Cornelia Rumpf-Kienzl[2], Mauro Delorenzi[10,12,13], Lodewyk Wessels[1], Ramon Salazar[14], Federica Di Nicolantonio[4,5], Alberto Bardelli[4,5], Jacco van Rheenen[3], René Medema[2], Sabine Tejpar[15] and René Bernards[1*]

[1]Division of Molecular Carcinogenesis, and Cancer Genomics Center Netherlands, The Netherlands Cancer Institute, Plesmanlaan 121, 1066 CX Amsterdam, The Netherlands

[2] Division of Cell Biology, The Netherlands Cancer Institute, Plesmanlaan 121, 1066 CX Amsterdam, The Netherlands

[3] Cancer Genomics Netherlands, Hubrecht Institute-KNAW & University Medical Center Utrecht, Uppsalalaan 8, 3584 CT Utrecht, the Netherlands

[4] Department of Oncology, University of Torino, SP 142, Km 3.95, 10060, Candiolo, Torino, Italy; FIRC Institute of Molecular Oncology (IFOM), 20139 Milano, Italy

[5] Candiolo Cancer Institute-FPO, IRCCS, SP142, Km 3.95, 10060 Candiolo, Italy

[6] FIRC Institute of Molecular Oncology (IFOM), 20139 Milano, Italy

[7] Program Against Cancer Therapeutic Resistance (ProCURE). Chemoresistance and Predictive Factors Group.Catalan Institute of Oncology (ICO), Bellvitge Institute for Biomedical Research (IDIBELL), L'Hospitalet del Llobregat, 08908 Barcelona, Spain

[8] Sanofi Oncology, 13 Quai Jules Guesde, 94403 Vitry sur Seine, France.

[9] Agendia, Science Park 406,1098 XH Amsterdam, The Netherlands

[10] Bioinformatics Core Facility, SIB Swiss Institute of Bioinformatics, Quartier Sorge - Batiment Genopode 1015 Lausanne, Switzerland

[11] Division of Molecular Pathology, The Netherlands Cancer Institute, Plesmanlaan 121, 1066 CX Amsterdam, The Netherlands

[12] Department of Oncology, University of Lausanne, Rue de Bugnon 21, 1011 Lausanne, Switzerland

[13] Ludwig Center for Cancer Research, University of Lausanne, Chemin des Boveresses 155, 1066 Epalinges, Switzerland

[14] Medical Oncology Department, Catalan Institute of Oncology, IDIBELL, Bellvitge Biomedical Research Institute, 08908 L'Hospitalet de Llobregat, Catalonia, Spain

[15] Molecular Digestive Oncology, University Hospitals Leuven and KU Leuven, Herestraat 49, 3000 Leuven, Belgium.

[#]These authors contributed equally to this work

Running title: A vulnerability of *BRAF*-like colon cancer

Keywords: BRAF-like colon cancer, functional genomics, RANBP2, vinorelbine, targeted treatment.

Financial support

This work was supported by grants from ESMO for Translational Research (LV), EU FP7 program grant COLTHERES (RB, FDN, AB, ST, IS, TS, GDA, ML), NWO grant CSBC (RLB, RB, LW and CL), the Dutch Cancer Society (KWF) (RB), the Fondo de Investigaciones Sanitarias PI13-01339) and Generalitat de Catalunya (2005SGR00727) (AV), *AIRC IG n. 12812 (AB); AIRC IG n. 17707 (FDN),* Fondazione Piemontese per la Ricerca sul Cancro-ONLUS 5 per mille 2010 e 2011 Ministero della Salute (AB, FDN), Fondo per la Ricerca Locale (ex 60%), Università di Torino, 2014 (FDN);

***Corresponding Author:**

Rene Bernards; email r.bernards@nki.nl; tel. +31-20 5126973

Conflict of interest

N.E-M., M. C., L. C., C. N., C. C. and C. H. are employees of Sanofi Oncology. IS and TS

were employees of Agendia at the time of the study.

SUMMARY

BRAF(V600E) mutant colon cancers (CCs) have a characteristic gene expression signature, which is also found in some tumors lacking this mutation. Collectively, they are referred to as "*BRAF*-like" tumors and represent some 20% of CCs. We used a shRNA-based genetic screen focused on genes upregulated in *BRAF(V600E)* CCs to identify vulnerabilities of this tumor subtype that might be exploited therapeutically. We identify here RANBP2 (also known as NUP358) as essential for survival of *BRAF*-like, but not for non-*BRAF*-like CC cells. Suppression of RANBP2 results in mitotic defects only in *BRAF*–like CC cells, which lead to cell death. Mechanistically, RANBP2 silencing reduces microtubule outgrowth from the kinetochores, thereby inducing spindle perturbations, providing an explanation for the observed mitotic defects. We find that *BRAF*-like CC display far greater sensitivity to the microtubule poison vinorelbine both *in vitro and in vivo*, suggesting that vinorelbine is a potential tailored treatment for *BRAF*-like CCs.

Statement of significance

The BRAF-like signature identifies *BRAF(V600E)* mutant colon cancers (CC) and a group of tumors lacking this mutation that share the same gene expression profile and the same poor prognosis. Through a shRNA-based genetic screen we identified RANBP2 to be lethal in cells having the BRAF-like gene signature.

RANBP2 loss in BRAF-like CC cells reduces microtubule outgrowth from the kinetochores. This causes a plethora of mitotic defects, leading to cell death. BRAF-like CC cells display an exquisite sensitivity to vinorelbine, suggesting vinorelbine as a targeted agent for BRAF-like CCs.

INTRODUCTION

Colorectal cancer (CRC) represents one of the most common cancers worldwide, with an estimated 1,2 million cases yearly and an annual mortality of over 600,000 (Jemal et al., 2011). Due to the relatively asymptomatic progression of the disease in the early stages, patients are frequently diagnosed with metastatic disease, with a five-year survival rate of around 10% (Cidón, 2010). BRAF is a protein kinase downstream of RAS in the RAS-RAF-MEK-ERK kinase pathway. V600E is the most common point mutation of the *BRAF* gene and is present in approximately 8-10% of the CRC patients (Tie et al., 2011; Yuan et al., 2013). Several reports have consistently shown the negative impact of *BRAF(V600E)* mutation on CRC prognosis, especially in the metastatic setting (Bokemeyer et al., 2011; Van Cutsem et al., 2011; Richman et al., 2009; Tol et al., 2009). *BRAF(V600E)* colon cancers (CCs) are characterized by a distinct and homogeneous gene expression profile when compared to *KRAS* mutant and *KRAS-BRAF* double wild type (WT2) CCs. (Popovici et al., 2012; Tian et al., 2013). This *BRAF* mutant gene expression signature identifies *BRAF* mutant tumors with high sensitivity (96%) and, when applied to *BRAF* WT CCs, it also identifies subsets of *KRAS* mutant (30%) and a subset of WT2 (13%) tumors. Tumors having this gene signature are referred to as "*BRAF*-like" and have a similar poor prognosis irrespective of the presence of the *BRAF(V600E)* mutation. The treatment of both early stage and metastatic cancer patients is mainly based on chemotherapy. Predictive biomarkers of response are required to help identifying the group of patients who might benefit from certain chemotherapeutic treatments and avoiding unnecessary toxicity for those who will not benefit. To date, very few predictive biomarkers for chemotherapy response have been identified and none of them are used in clinical practice (Glück et al., 2013; Roepman et al., 2013; Sargent, 2014; Sinicrope et al., 2011; Vollebergh et al., 2014).

Functional genetic screens represent a powerful tool to identify mechanisms of drug response and synthetic lethal interactions (Berns et al., 2007; Luo et al., 2009; Prahallad

et al., 2012; Steckel et al., 2012). We applied a loss of function genetic screen to identify vulnerabilities of *BRAF*-like colon cancer cells. Here we describe a specific Achilles heel of these cells that can be targeted by vinorelbine, a chemotherapeutic drug currently not used clinically for the treatment of colon cancer.

RESULTS

RANBP2 suppression is selectively lethal to *BRAF*-like colon cancers

To identify synthetic lethal interactions of *BRAF* mutant colon cancer, we performed a loss-of-function genetic screen in which we specifically focused on genes up-regulated in *BRAF(V600E)* CCs. We hypothesized that some of these genes may be selectively required to tolerate the presence of the *BRAF* mutation. We identified 363 genes that are overexpressed in *BRAF* mutant CCs as compared to *BRAF* and *KRAS* wild type (*WT2)* CCs using two gene expression data sets (Popovici et al., 2012; Tian et al., 2013) (Figure 1A, left panel). For each dataset, the genes overexpressed in *BRAF* mutant tumors were determined, using a cutoff of 0.05 on the Benjamini-Hochberg false discovery rate to control for multiple testing. We selected 163 genes common to both data sets as well as the top 100 of the remaining upregulated genes unique to each data set, yielding in total a set of 363 genes. The individual lists of genes are reported in Supplemental Table S1. We then selected 1586 shRNA vectors from the TRC shRNA collection (TRC-Hs1.0) to generate a sub-library targeting the 363 genes of interest ("BRAF library"). To identify those genes that are specifically lethal in *BRAF*(V600E) cells versus WT2 cells we selected three CC cell lines. WiDr and Vaco432 colon cancer cell lines harbor a *BRAF(V600E)* gene mutation and are defined as *BRAF*-like by gene expression signature. The LIM1215 colon cancer cell line is wild type for *KRAS* and *BRAF* genes (WT2) and is defined as non-*BRAF*-like by signature.

WiDr, Vaco432 and LIM1215 were infected with the BRAF shRNA library. The infected cells were selected for viral integration and cultured for 13 days, after which shRNAs were recovered by PCR (Figure 1A, right panel). The relative abundance of shRNA vectors was determined by next generation sequencing of the barcode identifiers present in each shRNA vector (Supplemental Table S2). We first considered shRNA vectors that were significantly depleted in *BRAF(V600E)* CC cells at day 13 as compared to day 0 by

at least 50% (log2 Time13/Time0 ≤ -1, p- adjusted value ≤ 0.1). Subsequently, we determined the fold depletion between *BRAF* mutant CC cells and LIM1215 cells and selected those shRNAs that had a ratio of more than 2 fold (WM fold change) ≥ 2). To increase the fidelity of the hits, genes represented by multiple shRNAs matching these criteria were prioritized (Supplemental Table S3). From this list we selected *RANBP2* represented by three individual shRNAs for further validation and follow-up. We tested all five *RANBP2* shRNAs present in the library in *BRAF(V600E)* cells and WT2 cells and confirmed the increased sensitivity of the *BRAF(V600E)* CC cells upon RANBP2 silencing as compared to WT2 CC cells (Supplemental Figure S1A and S1B). Based on their knockdown efficiency, shRNAs #1 and #3 were selected for further studies. In a second independent experiment, colony formation assays confirmed that silencing of *RANBP2* with shRNA#1 and #3 specifically impaired the proliferation of the two *BRAF* mutant (Vaco432 and WiDr) CC cell lines, but not the WT2 CC cell line LIM1215 (Figure 1B). This impairment correlated with cell death as shown by increased apoptosis (Figure 1C).

Since the genes tested in this genetic screen are not only upregulated in *BRAF* mutant CCs but also in the *BRAF*-like CCs, we also studied *RANBP2* suppression as a potential vulnerability in a larger panel of CC cell lines that are either *BRAF*-like or non-*BRAF*-like by gene signature. Cell lines were categorized as WT2, *BRAF(V600E) or KRAS* mutant based on mutation status and, based on gene expression, as *BRAF*-like or non-*BRAF* like. The proliferation of none of the 6 non-*BRAF*-like CC cell lines was impaired by *RANBP2* suppression, irrespective of *KRAS* mutation status. In contrast, proliferation of all 9 *BRAF*-like CC cell lines was dramatically inhibited upon *RANBP2* suppression, irrespective of *KRAS* and *BRAF* mutation status (Figures 1D and 1E). Microsatellite instability (MSI) status did not correlate with this phenotype either. The degree of *RANBP2* silencing is comparable across the different cell lines (Supplemental Figure S1C). The sensitivity observed in BRAF-like cells is related to the silencing of the gene rather than to an unspecific effect of the hairpins since no toxicity was observed, neither

with scrambled RANBP2 shRNA nor with pLKO as compared to parental lines (Supplemental Figure S1D). We conclude that *RANBP2* knockdown is selectively lethal for *BRAF*-like CC cell lines.

***RANBP2* knockdown causes mitotic abnormalities in *BRAF*-like cells.**

RANBP2 is a small GTP-binding protein belonging to the RAS superfamily and, as part of the nuclear pore complex, is a crucial regulator of nucleo-cytoplasmic transport. However, it also plays an important yet ill-defined role in kinetochore function during mitosis. RANBP2 silencing has been reported to be responsible for abnormal mitotic progression and abnormal chromosome segregation, eventually leading to mitotic catastrophe (Hashizume et al., 2013; Salina et al., 2003). We therefore asked whether *RANBP2* expression in *BRAF*-like colon cancer cells is required for mitotic progression. We performed time-lapse microscopy experiments in three different non-*BRAF*-like CC cells (LIM1215, Caco2 and HCT15) and three different *BRAF*-like CC cells (Vaco432, WiDr and HCT116) upon RANBP2 silencing. Cells were first transduced with GFP-tagged histone H2B (H2B-GFP) to allow visualization of the chromosomes in mitosis and then infected with RANBP2 shRNA #1 or #3 or control vector pLKO. Images were acquired every 10 minutes over a period of 72 hours. The degree of *RANBP2* silencing is shown in Supplemental Figure S2A. Figure 2A shows that for *BRAF*-like CC cells silencing of *RANBP2* resulted in a significant increase of the time spent in mitosis (2 times longer) as compared to pLKO-infected cells. In contrast, length of mitosis was only slightly increased (0.8 to 1.4 times longer) in non-*BRAF*-like CC cells upon *RANBP2* loss. Moreover, up to 75% of the mitosis events counted in *BRAF*-like *RANBP2* depleted CC cells displayed a range of defects, including delay in alignment, metaphase delay, spindle defects, anaphase bridges and lagging chromosomes (Supplemental Figure S2B). These abnormalities eventually lead to death during or straight after mitosis (Figure 2B). In contrast only few mitotic defects (2% in LIM1215, 4% in HCT15, and 6% in Caco2, respectively) were observed in non-*BRAF*-like CC cells. These results show

that *RANBP2* suppression induced cell death in *BRAF*-like CC cells is driven by defects in mitosis and identifies mitosis as a potential vulnerability of *BRAF*-like CC cell lines.

RANBP2 **knockdown affects microtubule dynamics in** ***BRAF*****-like cell lines.**

RANBP2 is part of the RANBP2-RANGAP1 complex. It has been shown to play a role in the interaction of kinetochores with kinetochore fibers and in regulating the function of kinetochores through its cyclophilin-like domain and E3 SUMO-ligase domain (Arnaoutov et al., 2005; Clarke, 2005). It was hypothesized that the interaction of the RANBP2-RANGAP1 complex with kinetochores can also regulate other effectors through localized GTP hydrolysis by RAN (Clarke and Zhang, 2008). RAN-regulated targets in mitosis include mostly microtubule stabilizing factors and factors involved in microtubule nucleation (Clarke and Zhang, 2008). We also observed several mitotic defects in *BRAF*-like CC cells upon *RANBP2* suppression, including spindle defects. To better evaluate whether any abnormalities in the microtubule (MT) nucleation could explain the essential mitotic role of RANBP2 in *BRAF*-like CC, we performed nocodazole washout experiments, a standard tool to study MT outgrowth from centrosomes and kinetochores. We first disassembled MTs by using high dose nocodazole for a short time period and, after removal of the drug, the initial stage of MT re-growth at both centrosomes and kinetochores was evaluated in a time course analysis. The first experiment was performed in a non-*BRAF*-like CC cell line (Caco2) and in a *BRAF*-like CC cell line (WiDr). Within 30 minutes of nocodazole removal both the non-*BRAF*-like CC cell line (Caco2) and the *BRAF*-like CC cell line (WiDr) showed an almost mature spindle, thus indicating the reversible action of the drug (Figure 3A and 3B). A robust microtubule growth from both centrosomes and kinetochores was observed in the non-*BRAF*-like CC cell line (Figure 3A), while a severe impairment of microtubule growth from kinetochores was observed in the *BRAF*-like CC cell line within the first 6 minutes of the time course (Figure 3B). To further characterize the robustness of this phenotype, we performed

nocodazole washout experiments in several CC cell lines previously categorized based on the *BRAF*-like status. As shown in Figure 3C, we did not observe any major differences in terms of MTs outgrowth from the centrosomes between *BRAF*–like and non-*BRAF*-like CC cells within the first 6 minutes of the time course. However, we observed a clear impairment of microtubule outgrowth from the kinetochores in *BRAF*-like CC cells compared to non-*BRAF*-like CC cells (Figure 3D) in the same time frame. Samples images for the categories used to score the outgrowth from both the centrosomes and the kinetochores are reported in Supplemental Figure S3A. Nucleation of MTs from kinetochores is regulated by the RAN gradient as well by the RANGAP1-RANBP2 complex (Clarke and Zhang, 2008; Torosantucci L, 2008). The impairment of MTs outgrowth from the kinetochores observed in *BRAF*-like CC cells could explain their dependency on RANBP2. We therefore asked what the role of RANBP2 is in MTs nucleation from the kinetochores in *BRAF*-like and non-*BRAF*-like CC. Two non-*BRAF*-like (Caco2 and HCT15) and two *BRAF*-like (WiDr and HCT116) CC cell lines were infected with the RANBP2 shRNAs #1 or #3 and pLKO as a control. After puromycin selection, cells were harvested and seeded for a nocodazole washout experiment. Three independent biological replicates were performed per cell line and the MTs outgrowth from both the centrosomes and the kinetochores was again scored within the first 6 minutes of nocodazole washout by using the same scoring methodology as described for Figure 3C, D. We considered the two cell lines in each group to belong to the same category. To increase statistical power we combined the results of the three independent replicate measurements of the two cell lines in each group. As shown in Figure 3E, neither the MTs outgrowth from the centrosomes nor the MT outgrowth from the kinetochores was perturbed in non-*BRAF*-like cell lines upon *RANBP2* knockdown. Interestingly, we found that *RANBP2* knockdown significantly decreased MTs outgrowth from the kinetochores in *BRAF*-like CC cell lines, as evidenced by the reduction of the "weak outgrowth" category ("+") and the increase of the "null-outgrowth" category ("-"). In particular, the weak outgrowth category dropped from 61% in controls to 34% with

shRNA #1 (Benjamini-Hochberg false discovery rate (FDR=0.08) and to 48% with shRNA #3 (FDR=0.5). The null outgrowth category increased from 18% in the pLKO condition to 57% with hairpin #1 (FDR=0.003) and to 41% with hairpin #3 (FDR=0.02). The analysis for the individual cell lines with the corresponding silencing is shown in Supplemental Figure S3B-F. These results show that silencing of *RANBP2* further reduces MT nucleation from the kinetochores, suggesting that *BRAF*-like CC tumors rely on *RANBP2* to compensate for an impairment of MTs nucleation from the kinetochores. This makes these tumors particularly vulnerable to loss of *RANBP2* expression. Indeed its loss triggers spindle perturbations that cause several mitotic defects, leading to cell death.

BRAF-like colon cancer cells are sensitive to vinorelbine

Our findings that *RANBP2* loss perturbs spindle formation, prolongs the time spent in mitosis, triggers several mitotic defects and ultimately induces death during or immediately after mitosis raises the possibility that *BRAF*-like CC cells are vulnerable to mitotic spindle poisons that act on microtubule dynamics. To address this, we mined the data from the Genomics of Drug Sensitivity in Cancer project (Sanger Panel) to see if *BRAF(V600E)* CC cell lines are more sensitive to mitotic drugs as compared to WT2 CC cell lines (Garnett et al., 2012). Data were available for a total of 15 CC cell lines that were tested for sensitivity to both vinca alkaloid compounds (vinorelbine, vinblastine) and taxanes (paclitaxel and docetaxel). As shown in Figure 4A, no significant difference in sensitivity was observed for vinblastine (Wilcoxon test p-value=0.85), paclitaxel (p-value=0.13) and docetaxel (p-value=0.2). *BRAF(V600E)* CC lines, however, were significantly more sensitive to vinorelbine than WT2 CC cells (p-value=0.04) with a difference of over 30-fold in the median IC50 values. To further validate these findings we treated a panel of 22 colon cancer cell lines for 72 hours with different concentrations of vinorelbine, vinblastine and paclitaxel. Our cell lines were previously profiled for gene expression to define their BRAF-like status and were homogeneously distributed among the two categories, (11 BRAF-like and 11 non BRAF-like cell lines). As reported in Figure

4B, we also observed a significant difference in sensitivity to vinblastine and paclitaxel in BRAF-like cells as compared to non BRAF-like cells, in contrast with what was observed in the Sanger panel. This could be explained by the relatively small number of cells tested in the Sanger panel. Despite of its statistical significance, the difference observed in the median IC50 values for paclitaxel is only about 2-fold, while for vinorelbine and vinblastine is more than 100-fold (Supplemental Table S4).

To corroborate the sensitivity of BRAF-like CC cells to the vinca alkaloid compounds, we treated the same panel of CC cell lines with vinorelbine, vinblastine and paclitaxel for about 2 weeks in colony formation assays. Figure 4C-F shows that the lethal concentration of vinorelbine for non BRAF-like CC cells ranged between 10nM and >100nM while BRAF-like CC cells showed a lethal dose ranging between 0.01nM and 1nM. This means that *BRAF*-like CC cells were 10 to 10,000 fold more sensitive to vinorelbine compared to non BRAF-like. The differences observed with paclitaxel were more limited (about 2-fold, data not shown), while vinblastine showed a difference of 10 to 100 fold (Supplemental Figure S4A-B). These results confirmed the specific vulnerability of *BRAF*-like CC cell lines to vinorelbine as also observed in the Sanger cell line data set and in our short terms assays. The exquisite sensitivity of *BRAF*-like CC cells lines to vinorelbine was not related to an increased proliferation rate since the proliferation rate of *BRAF*-like CC cell lines was not significantly different from that of non-*BRAF*-like cell lines (Supplemental Figure S4C). Importantly, *BRAF(V600E)* CC cells lines had an IC50 for vinorelbine that was similar to that of breast and lung cancer cell lines, two solid tumors for which vinorelbine is used in clinical practice (Supplemental Figure S4D).

To further characterize the vulnerability of *BRAF*-like CC to vinorelbine, H2B-YFP expressing CC cells were analyzed by time-lapse microscopy upon vinorelbine treatment (10nM) over 72 hours. As reported in Figure 4G, while non BRAF-like CC cells were dividing over a period of 24 hours of observation upon vinorelbine treatment, *BRAF*-like CC cells were mainly arrested in mitosis, with a percentage of cells dying during mitosis

or slipping out of mitosis followed by cell death. After 72 hours of vinorelbine treatment, non BRAF-like CC cells were still dividing with a minor percentage of cells dying and slipping out of mitosis, while *BRAF*-like CC were mainly dead with a minor percentage of cells still arrested in mitosis (Figure 4H). These findings were further confirmed by western blot analysis. We observed an arrest in M-phase with an increase of the cyclin B1 levels after 24-48 hours of treatment and in some cases after 12 hours followed by apoptosis in *BRAF*-like CC cells (Supplemental Figures S4E) while we only observed a slight increase of cyclin B1 with mild apoptosis in HCT15 (non BRAF-like) and a slight increase of apoptosis in LIM1215 (non BRAF-like) over a period of 72 hours treatment.

In vivo effects of vinorelbine

To assess whether the in vitro findings can be recapitulated in vivo, Vaco432 and RKO (*BRAF*(*V600E*) BRAF-like), HCT116 (*KRAS* mutant BRAF-like), SW480 and HCT15 (*KRAS* mutated non *BRAF*-like) CC cells were injected in nude mice. Upon tumor establishment (200-250 mm^3), xenografts were treated with either vehicle or vinorelbine (10mg/kg) for 40-50 days. Vinorelbine treatment significantly impaired tumor growth of *BRAF* mutated (Vaco432) and *BRAF*-like (HCT116) xenografts, while no antitumor effect was observed in non-*BRAF*-like (SW480 and HCT15) mice (Figure 5A-D). While RKO cells were very sensitive to vinorelbine in vitro (Figure 4D) and to RANBP2 silencing (SupplementalFigure S5A), no effect was observed in RKO xenografts (Figure 5E). This suggests that drug response in vivo can be modulated by factors from the local microenvironment. In particular TGFβ can lead to powerful resistance to a number of cancer drugs, including chemotherapy (Brunen et al., 2013; Huang et al., 2012). To test whether RKO cells are sensitive to TGFβ induced drug resistance, we exposed RKO cells to recombinant TGFβ in cell culture. Recombinant TGFβ increased phosphorylation of SMAD2, a sign of active TGFβ signaling and induced a more than 100-fold increase in IC50 for vinorelbine (Figure S5B-E). To replicate the original anatomic site of colorectal

cancer we further validated our findings by orthotopic tumor implanting in mice. Two non *BRAF*-like CC cell lines, Caco2 and HCT15, (Figure 5F-G) and 2 *BRAF*-like CC cell lines, WiDr and HCT116, (Figure 5H-I) were used for the generation of orthotopic engrafted tumors to measure the response to vinorelbine (see Extended Experimental procedures). As shown in Figure 5F and G, both Caco2 and HCT15 orthotopically implanted tumors did not respond to vinorelbine treatment, while both WiDr and HCT116 orthotopically implanted tumors significantly responded to vinorelbine (Figure 5H-I). Taken together, these experiments indicate that most *BRAF*-like CC tumors also have increased sensitivity to vinorelbine in vivo.

Response to vinorelbine of liver implanted colon cancer cell lines

The first site of metastatic dissemination of colon cancer is often the liver. Since new drugs are tested initially in the metastatic setting, we tested whether vinorelbine is active against colon cancer cells growing in the liver. We injected CC cells into the liver of NOD scid gamma mice and filmed them using intravital imaging upon vinorelbine treatment. We filmed the same imaging areas of CC liver implantation before, 24hrs and 48hrs post vinorelbine/vehicle treatment with subcellular resolution through an abdominal imaging window as we described recently (Ritsma et al., 2012, 2013) (Figure 6A). The CC cells expressed a chimera of H2B tagged and photo-switchable Dendra2 (H2B-Dendra2). The visualization of chromosome condensation by the fluorescent tag was used to identify mitotic status and apoptotic bodies, and the green-to-red Dendra2 photo-marking of imaging fields was used to retrace the imaging areas in subsequent imaging sessions (Figure 6A) (Janssen et al., 2013). Before treatment and during vehicle treatment (Supplemental Figure S6A), only a few mitotic figures were observed in both the *BRAF*-like SNU-C5 cells and the non-*BRAF*-like Caco2 cells. Strikingly, when we imaged the same imaging field 24hrs after vinorelbine treatment, we observed a remarkable increase in mitotic figures and cell fragments in the *BRAF*-like cells implanted into the liver, but not in the non-*BRAF*-like cells growing in the liver (Figure 6B). In the next 24hrs, the number

of cell fragments increased with a concomitant decrease in the number of mitotic figures (Figure 6B). These data were fully consistent with our model that *BRAF*-like cells are more sensitive to vinorelbine and that the toxicity is due to a mitotic arrest followed by apoptosis. Moreover, these data suggest that liver metastases of BRAF-like colon cancers also respond to vinorelbine therapy.

***BRAF(V600E)* as predictive biomarker of DM4 response in CC PDX models.**

DM4 is a potent cytotoxic agent derived from maytansine that blocks tubulin polymerization and interferes with the binding of vinblastine to tubulin, indicating a common mechanism of action (Prota et al., 2014). We therefore asked whether the sensitivity of response of CC Patient-derived xenograft (PDX) to DM4 would also be predicted by BRAF mutation status. Intrinsic sensitivity to DM4 of the PDX models was determined by the antitumor efficacy of a single high dose (40mg/kg) of a non-targeting antibody (directed against human CD19, unable to bind mouse CD19) conjugated to DM4 in tumor-bearing mice (see extended experimental procedures).

PDX sensitivity to the non tumor-targeting antibody DM4 conjugate varied with 11/20 PDX models displaying lack of sensitivity and 9/20 displaying intrinsic sensitivity (Supplemental Table S5). Examples of DM4-sensitive and resistant PDX models are shown in Figure S6B-C. Interestingly the *BRAFV600E* activating mutation was found exclusively in DM4-sensitive models (Figure 6C). Indeed 44% of CC PDX responders carry the *BRAF(V600E)* mutation, while none of the non-responders carry the same BRAF activating mutation (Fisher exact test p-value= 0.026). Taken together these data strengthen our finding of microtubules dynamic to be a specific target of BRAFV600E and eventually BRAF-like CC.

Complete remission of a BRAF-like colon cancer patient with vinca alkaloids.

A study report was published in 1994, in which 15 metastatic CC patients were treated with vinblastine in combination with bepridil to investigate if a calcium channel blocker

could overcome the multi drug resistance to vinblastine. The overall study was negative, but one out of 15 patients received a complete remission which lasted over 20 years after repeated cycles of therapy with vinblastine-containing regimen (Linn et al., 1994). We retrieved the primary tumor of the patient and performed both DNA and RNA extraction to look for mutations in *KRAS*, *NRAS* and *BRAF* genes and determine BRAF-like status by gene expression profiling. The sequence data revealed that the tumor carried a *KRAS* mutation. Gene expression analysis revealed the tumor to be BRAF-like (Figure 6D). This super responder patient further supports the notion that BRAF-like CC are responsive to vinca alkaloids.

Discussion

Oncogenomic studies have enabled a molecular taxonomy of colorectal cancer (Ana Sebio, 2015; Dienstmann, 2014), but to date, this has had only a limited impact on the clinical management of this disease. *BRAF(V600E)* mutations occur in about 8-10% of CRC patients and are associated with a poor prognosis, especially in the metastatic setting (Bokemeyer et al., 2011; Van Cutsem et al., 2011; Richman et al., 2009; Tol et al., 2009). These tumors can be identified by a distinctive gene expression signature. This signature reliably identifies tumors with *BRAF(V600E)* mutation and a set of tumors lacking a *BRAF* mutation. We collectively refer to the CC tumors with this *BRAF* gene signature as "*BRAF*-like". In addition to their similar gene expression profile, they are also characterized by similarly poor prognosis (Popovici et al., 2012; Tian et al., 2013). To identify additional vulnerabilities of these tumors that can be exploited therapeutically, we used a loss-of-function genetic approach. We identified *RANBP2* as an essential gene for BRAF-like CC cell lines. RANBP2 belongs to the RAS superfamily and is a major cytosolic component of filaments that derives from the cytoplasmic ring of the nuclear pore complex. More recently, RANBP2 and the RANBP2-RANGAP1 complex have been shown to play an important role in mitosis. In particular RANBP2 has a role in the interaction of kinetochores with the microtubule bundles that extend from the centrosomes to the kinetochores (Clarke and Zhang, 2008; Joseph, 2004). Depletion of RANBP2 by RNAi causes defective kinetochore structure and composition, abnormal mitotic progression and abnormal chromosome segregation (Joseph et al., 2002; Salina et al., 2003). In agreement with these reports, we observed several mitotic defects in *BRAF*-like CC cells upon *RANBP2* knockdown, in particular prolonged mitosis eventually triggering cell death. The percentage of dead cells observed during the time-lapse experiment is a function of the observation time (72hrs). Hence, the colony formation assays (performed over a 10 days period) result in more significant cell death.

The RAN-GTP gradient is important for the stabilization and nucleation of microtubules around kinetochores (Arnaoutov and Dasso, 2003). RAN-GTP binds importin-ß and

releases factors that are involved in spindle assembly (Clarke and Zhang, 2008), and its localization at kinetochores requires RANBP2. We found *BRAF*–like CC cell lines to be defective in the microtubule outgrowth from kinetochores and RANBP2 depletion to further reduce this microtubule outgrowth. We therefore hypothesize that RANBP2 allows BRAF-like CC cells to tolerate such a defect. Consequently, RANBP2 depletion results in cell death.

The specific defect of *BRAF*-like cells in microtubule formation unveiled a potential vulnerability of such tumors to microtubule disrupting agents. Indeed, we found that *BRAF*-like CC cells were 10 to 10,000-fold more sensitive to vinorelbine than non-*BRAF*-like CC cells. Moreover, we tested 5 *BRAF*-like and 3 non-*BRAF*-like colon cancer cells in various in vivo animal models for their sensitivity to vinorelbine. All but one cell line reacted in accordance to their gene expression profile: the *BRAF*-like being far more responsive than their non-*BRAF*-like counterparts (Figures 5 and 6). Furthermore, in a series of 20 patient derived xenograft (PDX) models of colon cancer, we found that *BRAF(V600E)* mutation is a predictive biomarker of response to DM4, a potent anti-mitotic agent with a mechanism of action similar to vinca alkaloids.

Vinorelbine has been rarely used for the treatment of colon cancer. Only three studies have been reported (Gebbia et al., 1996; Iaffaioli et al., 1995; Linn et al., 1994). The tumor of one patient who got a complete and lasting remission after vinblastine treatment could be retrieved (Linn et al., 1994). The analysis of the sample revealed the tumor to be BRAF-like by gene expression (Figure 6D). While super-responders are rare, they can point at particular biomarkers that can be used to identify patient subsets likely to benefit from specific treatment. In this particular case, the identification of this patient as BRAF-like provides an incentive to test vinorelbine in this patient group, which represents some 20% of all colon cancers. However, we cannot exclude that other factors not present in our current models will modulate clinical responses to vinorelbine. A clinical study to assess the utility of vinorelbine in *BRAF*-like colon cancer is scheduled to start in the near future. Our data also suggest that *BRAF*-like CCs are attractive subtypes to target

with maytansine-derived antibody drug conjugates. More generally, our findings highlight the utility of functional genetic approaches to find vulnerabilities of subgroups of cancers that can be exploited in the clinic.

Methods

Selection of the genes used for the *BRAF*-like shRNA library.

Genes overexpressed in *BRAF(V600E)* tumors as compared to *BRAF* and *KRAS* wild type (*WT2)* tumors from two gene expression data sets were used: Popovici et al., 2012 and Tian et al. 2013. Genes were filtered according to variability by selecting only those features for which the difference between the 95th and the 5th percentiles was greater than 0.5 log2-units Differential expressed genes were identified with the limma package for the R statistical software (Ritchie et al., 2015). The Benjamini-Hochberg false discovery rate (FDR) was used to control for multiple hypothesis testing, with the cutoff for statistical significance set at 0.05.

Synthetic Lethal shRNA screen

The pooled shRNA dropout screen adapted from Prahallad et al., 2012 is described in Supplemental Experimental Procedures

Cell Culture, Viral Transduction.

Experiments were performed as described by Prahallad et al., 2012. See the Supplemental Experimental Procedures for details.

Long-Term Proliferation Assays

For loss of function assays, after puromycin selection cells were seeded into 6-well plates (DiFi and SKCO-1 5x10^4 cells/well; all the other CC cell lines 2x10^4 cells/well) and cultured for 10 days. For vinorelbine and vinblastine treatments, cells were seeded into 6-well plates (DiFi, SKCO-1 and HDC54 5x10^4 cells/well; all the other CC cell lines 2x10^4 cells/well) and cultured both in the absence and presence of drugs as indicated. At the endpoints of colony formation assays, cells were fixed, stained with crystal violet and photographed. All knockdown experiments were done by lentiviral infection. All relevant assays were performed independently at least three times.

Time lapse microscopy and immunofluorescence

Time-lapse experiments and immunofluorescence were adapted from Raaijmakers et al., 2009 and Tanenbaum et al., 2010. See the Supplemental Experimental Procedures for details.

Author contributions

L.V., V.G., S.T., R.L.B. designed the screening. I.S., T.S., G.DA., M.D., L.V., V.G., S.T., R.L.B. generated the list of genes. R.L.B. and C.L. assisted with the screen analysis and hit selection. L.V., V.G., R.B designed experiments and L.V. and V.G performed them. J.R. and R.H.M. supervised the mitotic experiments. A.S. performed data analysis. M.R., A.B., F.D.N., A.B. supervised and/or performed the xenografts experiments. A.V. and D.M. performed the orthotropic models experiments. A.F., E.B. and J.V.R. performed the intravital imaging. S.M. helped for the revision of the manuscript. N.E.M., M.C., L.C., C.N., C.C. and C.H. provided the CC PDX models data. S.L. provided the patient's sample. S.I.V., T.S. performed the BRAF-call for the patient. L.V., V.G. and R.B. wrote the manuscript. All the authors read, revised and approved the manuscript. R.B. supervised the work.

Acknowledgements

We thank the members of the NKI Genomics Core Facility, the Pathology Department, Lauren Oomen and Lenny Brocks from the NKI Digital Microscopy Facility for technical support. We thank the members of the IDIBELL animal core facility for the mouse care. We are grateful to Astrid Bosma, Paul van der Valk, Jan Schellens, Michiel Boekhout, Erik Voets, Roy van Heesbeen, Magali Michaut, Rob Wolthuis for discussions and to Lydia Blot, Sukhvinder Sidhu and Véronique Blanc at Sanofi for their support. We would also thank John Lambert and Immunogen's colleagues for their contribution to the CC PDX work.

References

Ana Sebio, H.-J.L. (2015). The molecular taxonomy of colorectal cancer: what's new? Curr. Colorectal Cancer Rep. *11*, 118–124.

Arnaoutov, A., and Dasso, M. (2003). The Ran GTPase regulates kinetochore function. Dev. Cell *5*, 99–111.

Arnaoutov, A., Azuma, Y., Ribbeck, K., Joseph, J., Boyarchuk, Y., Karpova, T., McNally, J., and Dasso, M. (2005). Crm1 is a mitotic effector of Ran-GTP in somatic cells. Nat. Cell Biol. *7*, 626–632.

Berns, K., Horlings, H.M., Hennessy, B.T., Madiredjo, M., Hijmans, E.M., Beelen, K., Linn, S.C., Gonzalez-Angulo, A.M., Stemke-Hale, K., Hauptmann, M., et al. (2007). A Functional Genetic Approach Identifies the PI3K Pathway as a Major Determinant of Trastuzumab Resistance in Breast Cancer. Cancer Cell *12*, 395–402.

Bokemeyer, C., Bondarenko, I., Hartmann, J.T., de Braud, F., Schuch, G., Zubel, a., Celik, I., Schlichting, M., and Koralewski, P. (2011). Efficacy according to biomarker status of cetuximab plus FOLFOX-4 as first-line treatment for metastatic colorectal cancer: The OPUS study. Ann. Oncol. *22*, 1535–1546.

Brunen, D., Willems, S.M., Kellner, U., Midgley, R., Simon, I., and Bernards, R. (2013). TGF-β: An emerging player in drug resistance. Cell Cycle *12*, 2960–2968.

Cidón, E. (2010). The challenge of metastatic colorectal cancer. Clin. Med. Insights. Oncol. *4*, 55–60.

Clarke, P.R. (2005). The Crm de la crème of mitosis. Nat. Cell Biol. *7*, 551–552.

Clarke, P.R., and Zhang, C. (2008). Spatial and temporal coordination of mitosis by Ran GTPase. Nat. Rev. Mol. Cell Biol. *9*, 464–477.

Van Cutsem, E., Köhne, C.-H., Láng, I., Folprecht, G., Nowacki, M.P., Cascinu, S., Shchepotin, I., Maurel, J., Cunningham, D., Tejpar, S., et al. (2011). Cetuximab plus irinotecan, fluorouracil, and leucovorin as first-line treatment for metastatic colorectal cancer: updated analysis of overall survival according to tumor KRAS and BRAF mutation status. J. Clin. Oncol. *29*, 2011–2019.

Dienstmann, R. (2014). Colorectal Cancer Subtyping Consortium (CRCSC) identification of a consensus of molecular subtypes. p. 32:3511.

Garnett, M.J., Edelman, E.J., Heidorn, S.J., Greenman, C.D., Dastur, A., Lau, K.W., Greninger, P., Thompson, I.R., Luo, X., Soares, J., et al. (2012). Systematic identification of genomic markers of drug sensitivity in cancer cells. Nature *483*, 570–575.

Gebbia, V., Maiello, E., Testa, A., Cannata, G., Colucci, G., and Gebbia, N. (1996). Single agent vinorelbine in the treatment of unresectable lung metastases from colorectal cancer. Oncol. Rep. *3*, 563–565.

Glück, S., De Snoo, F., Peeters, J., Stork-Sloots, L., and Somlo, G. (2013). Molecular

subtyping of early-stage breast cancer identifies a group of patients who do not benefit from neoadjuvant chemotherapy. Breast Cancer Res. Treat. *139*, 759–767.

Hashizume, C., Kobayashi, a, and Wong, R.W. (2013). Down-modulation of nucleoporin RanBP2/Nup358 impaired chromosomal alignment and induced mitotic catastrophe. Cell Death Dis. *4*, e854.

Huang, S., Hölzel, M., Knijnenburg, T., Schlicker, A., Mcdermott, U., Garnett, M., Grernrum, W., Sun, C., Prahallad, A., Groenendijk, F.H., et al. (2013). Europe PMC Funders Group MED12 Controls the Response to Multiple Cancer Drugs through Regulation of TGF-β Receptor Signaling. Cell *151*, 937–950.

Iaffaioli, R., Facchini, G., Tortoriello, A., Caponigro, F., Gesue, G., Finizio, A., Dimartino, N., Desena, G., Antonelli, B., Scaramellino, G., et al. (1995). A phase-ii trial of 5-Fluorouracil, folinic Acid, vinorelbine in pretreated patients with metastic colorectal-cancer. Oncol. Rep. *2*, 513–516.

Janssen, A., Beerling, E., Medema, R., and van Rheenen, J. (2013). Intravital FRET Imaging of Tumor Cell Viability and Mitosis during Chemotherapy. PLoS One *8*.

Jemal, A., Bray, F., Center, M.M., Ferlay, J., Ward, E., and Forman, D. Global cancer statistics. CA. Cancer J. Clin. *61*, 69–90.

Joseph, J. (2004). The RanGAP1-RanBP2 Complex Is Essential for Microtubule-Kinetochore Interactions In Vivo. Curr. Biol. *14*, 611–617.

Joseph, J., Tan, S.H., Karpova, T.S., McNally, J.G., and Dasso, M. (2002). SUMO-1 targets RanGAP1 to kinetochores and mitotic spindles. J. Cell Biol. *156*, 595–602.

Linn, S.C., Giaccone, G., and Pinedo, H.M. (1994). Complete remission of metastatic colorectal cancer: a pitfall in a multidrug resistance reversal trial. Lancet *343*, 1648–1649.

Luo, J., Emanuele, M.J., Li, D., Creighton, C.J., Schlabach, M.R., Westbrook, T.F., Wong, K.K., and Elledge, S.J. (2009). A Genome-wide RNAi Screen Identifies Multiple Synthetic Lethal Interactions with the Ras Oncogene. Cell *137*, 835–848.

Popovici, V., Budinska, E., Tejpar, S., Weinrich, S., Estrella, H., Hodgson, G., Van Cutsem, E., Xie, T., Bosman, F.T., Roth, A.D., et al. (2012). Identification of a poor-prognosis BRAF-mutant - Like population of patients with colon cancer. J. Clin. Oncol. *30*, 1288–1295.

Prahallad, A., Sun, C., Huang, S., Di Nicolantonio, F., Salazar, R., Zecchin, D., Beijersbergen, R.L., Bardelli, A., and Bernards, R. (2012). Unresponsiveness of colon cancer to BRAF(V600E) inhibition through feedback activation of EGFR. Nature *483*, 100–103.

Prota, A.E., Bargsten, K., Diaz, J.F., Marsh, M., Cuevas, C., Liniger, M., Neuhaus, C., Andreu, J.M., Altmann, K.-H., and Steinmetz, M.O. (2014). A new tubulin-binding site and pharmacophore for microtubule-destabilizing anticancer drugs. Proc. Natl. Acad. Sci. U. S. A. 1–5.

Raaijmakers, J. a, Tanenbaum, M.E., Maia, A.F., and Medema, R.H. (2009). RAMA1 is a novel kinetochore protein involved in kinetochore-microtubule attachment. J. Cell Sci.

122, 2436–2445.

Richman, S.D., Seymour, M.T., Chambers, P., Elliott, F., Daly, C.L., Meade, A.M., Taylor, G., Barrett, J.H., and Quirke, P. (2009). KRAS and BRAF mutations in advanced colorectal cancer are associated with poor prognosis but do not preclude benefit from oxaliplatin or irinotecan: results from the MRC FOCUS trial. J. Clin. Oncol. *27*, 5931–5937.

Ritchie, M.E., Phipson, B., Wu, D., Hu, Y., Law, C.W., Shi, W., and Smyth, G.K. (2015). limma powers differential expression analyses for RNA-sequencing and microarray studies. *43*.

Ritsma, L., Steller, E.J. a., Beerling, E., Loomans, C.J.M., Zomer, a., Gerlach, C., Vrisekoop, N., Seinstra, D., van Gurp, L., Schafer, R., et al. (2012). Intravital Microscopy Through an Abdominal Imaging Window Reveals a Pre-Micrometastasis Stage During Liver Metastasis. Sci. Transl. Med. *4*, 158ra145–ra158ra145.

Ritsma, L., Steller, E.J. a, Ellenbroek, S.I.J., Kranenburg, O., Borel Rinkes, I.H.M., and van Rheenen, J. (2013). Surgical implantation of an abdominal imaging window for intravital microscopy. Nat. Protoc. *8*, 583–594.

Roepman, P., Schlicker, A., Tabernero, J., Majewski, I., Tian, S., Moreno, V., Snel, M.H., Chresta, C.M., Rosenberg, R., Nitsche, U., et al. (2013). Colorectal cancer intrinsic subtypes predict chemotherapy benefit, deficient mismatch repair and epithelial-to-mesenchymal transition. Int. J. Cancer *134*, 552–562.

Salina, D., Enarson, P., Rattner, J.B., and Burke, B. (2003). Nup358 integrates nuclear envelope breakdown with kinetochore assembly. J. Cell Biol. *162*, 991–1001.

Sargent, D.J. (2014). Prognostic impact of deficient mismatch repair (dMMR) in 7,803 stage II/III colon cancer (CC) patients (pts): A pooled individual pt data analysis of 17 adjuvant trials in the ACCENT database. J Clin Oncol *32:5s,*.

Sinicrope, F. a., Foster, N.R., Thibodeau, S.N., Marsoni, S., Monges, G., Labianca, R., Yothers, G., Allegra, C., Moore, M.J., Gallinger, S., et al. (2011). DNA mismatch repair status and colon cancer recurrence and survival in clinical trials of 5-fluorouracil-based adjuvant therapy. J. Natl. Cancer Inst. *103*, 863–875.

Steckel, M., Molina-Arcas, M., Weigelt, B., Marani, M., Warne, P.H., Kuznetsov, H., Kelly, G., Saunders, B., Howell, M., Downward, J., et al. (2012). Determination of synthetic lethal interactions in KRAS oncogene-dependent cancer cells reveals novel therapeutic targeting strategies. Cell Res. *22*, 1227–1245.

Tanenbaum, M.E., Vallenius, T., Geers, E.F., Greene, L., Mäkelä, T.P., and Medema, R.H. (2010). Cyclin G-associated kinase promotes microtubule outgrowth from chromosomes during spindle assembly. Chromosoma *119*, 415–424.

Tian, S., Simon, I., Moreno, V., Roepman, P., Tabernero, J., Snel, M., van't Veer, L., Salazar, R., Bernards, R., and Capella, G. (2013). A combined oncogenic pathway signature of BRAF, KRAS and PI3KCA mutation improves colorectal cancer classification and cetuximab treatment prediction. Gut *62*, 540–549.

Tie, J., Gibbs, P., Lipton, L., Christie, M., Jorissen, R.N., Burgess, A.W., Croxford, M., Jones, I., Langland, R., Kosmider, S., et al. (2011). Optimizing targeted therapeutic development: Analysis of a colorectal cancer patient population with the BRAFV600E mutation. Int. J. Cancer *128*, 2075–2084.

Tol, J., Nagtegaal, I.D., and Punt, C.J. a (2009). BRAF mutation in metastatic colorectal cancer. N. Engl. J. Med. *361*, 98–99.

Torosantucci L (2008). Localized RanGTP Accumulation Promotes Microtubule Nucleation at Kinetochores in Somatic Mammalian Cells. Mol. Biol. Cell *19*, 1873–1882,.

Vollebergh, M. a, Lips, E.H., Nederlof, P.M., Wessels, L.F., Wesseling, J., Vd Vijver, M.J., de Vries, E.G., van Tinteren, H., Jonkers, J., Hauptmann, M., et al. (2014). Genomic patterns resembling BRCA1- and BRCA2-mutated breast cancers predict benefit of intensified carboplatin-based chemotherapy. Breast Cancer Res. *16*, R47.

Yuan, Z.-X., Wang, X.-Y., Qin, Q.-Y., Chen, D.-F., Zhong, Q.-H., Wang, L., and Wang, J.-P. (2013). The prognostic role of BRAF mutation in metastatic colorectal cancer receiving anti-EGFR monoclonal antibodies: a meta-analysis. PLoS One *8*, e65995.

Figure legends

Figure 1. Identification and validation of *RANBP2* synthetic lethality with *BRAF*-like phenotype in colon cancer.

(A) *BRAF(V600E)* specific upregulated genes are used to assemble the BRAF library and perform a “dropout” shRNA screening.

Left panel: example of a heat map of BRAF activating 58-gene signature across 381 colon tumor samples of one of the two datasets considered (Tian S et al, Gut 2013). Tumors are sorted according to the signature scores. Upper row: tumors with BRAF(V600E) oncogenic mutations as measured by sequence analysis are indicated by black boxes, tumors without BRAF(V600E) oncogenic mutations are indicated by white boxes. Lower row: Tumors sharing the gene expression pattern of BRAF oncogenic mutation as measured by the signature are displayed as black boxes (BRAF-like subgroup), while tumors that share the gene expression pattern of BRAF-wild type are displayed as white boxes. The BRAF-like subgroup includes tumors with V600E mutation, tumors with KRAS mutation and tumors wild type for KRAS and BRAF

Right panel: schematic outline of the “dropout” shRNA screen for genes whose inhibition is selectively lethal in *BRAF*-like CC cell lines. After selecting 363 upregulated genes in BRAF(V600E) CCs tumors from the two datasets, the BRAF library was generated. Two *BRAF(V600E)* CC cell lines, Vaco432 and WiDr, were infected with the BRAF shRNA library polyclonal virus and screened for shRNAs that cause lethality. LIM1215 CC cell line (WT2) was used as a control.

(B-D-E) RANBP2 is synthetically lethal with *BRAF*-like phenotype in CC cells.

WT2 CC cells (LIM1215, Caco2, HCA7, Difi), *BRAF(V600E)* CC cells (WiDr, Vaco432, RKO, SNU-C5, SW1417, OXCO-1), *KRAS* mutant non-*BRAF*-like CC cells (HCT15, LIM1863) and *KRAS* mutant *BRAF*-like CC cells (SKCO-1, LoVo, HCT116) were stably infected with two independent shRNAs targeting *RANBP2* (sh*RANBP2* #1, sh*RANBP2* #3). Viability was assessed by colony formation assay. The pLKO vector was used as control. Cells were fixed, stained and photographed after 10 days of culture.

(C) The level of knockdown of RANBP2 protein and apoptosis induction was measured by western blot. See also Figure S1, Table S1, Table S2 and Table S3

Figure 2. *RANBP2* knockdown affects mitosis and induces cell death selectively in *BRAF*-like CC cell lines.

(A) *RANBP2* knockdown increases mitosis length in *BRAF*-like CC cells. H2B-GFP non *BRAF*-like CC cells (LIM1215, Caco2, HCT15) and H2B-GFP BRAF -like CC cells (Vaco432, WiDr, HCT116) were stably infected with 2 different shRNAs targeting *RANBP2* (shRANBP2#1, shRANBP2#3) and observed by time-lapse microscopy. For each CC cell line pLKO was used as negative control. The length (A) and the faith of mitosis (B) were assessed. Data are represented as mean ± standard error of mean (SEM). The p-value was calculated versus the pLKO-infected group (unpaired t-test with equal SD). The average number of mitosis evaluated per condition was 50.

(B) *RANBP2* knockdown induces death during or directly after mitosis selectively in *BRAF*-like CC cells. Graphic representation of cellular death quantification occurring

during mitosis or immediately after mitosis (within 3 hours from cytokinesis). The y-axis indicates percentage of cells showing no cell death, death during mitosis and death after mitosis. See also Figure S2A and S2B

Figure 3. *BRAF*-like CC cells have less microtubule nucleation from kinetochores that is further reduced by *RANBP2* knockdown (A) Representative images of MT outgrowth after nocodazole washout in Caco2 (non BRAF-like CC cell line) and WiDr (BRAF-like CC cell line) (B). Scale bars indicate 10 μm. Cells were stained for α tubulin to visualize MTs, CREST to visualize the kinetochores and DAPI to visualize the DNA. See extended supplemental procedures for details.

(C) Quantification of microtubule outgrowth at the centrosomes or at the kinetochores (D) in non-*BRAF*-like (Lim1215, Caco2, HCT15) and *BRAF*-like CC cell lines (RKO, Vaco432, WiDr, SNU-C5, HCT116, LoVo). The y-axis indicates the two groups of cells and the x-axis indicates the percentage of cells showing no ("-"), weak ("+"), medium ("++") or strong ("+++") microtubule outgrowth.

(E, F) Quantification of microtubule outgrowth from kinetochores or centrosomes in non-*BRAF*-like (E) (Caco2, HCT15) and *BRAF*-like cell lines (F) (WiDr, HCT116) upon *RANBP2*^{KD}. The y-axis indicates percentage of cells showing no ("-"), weak ("+"), medium ("++") or strong ("+++") microtubule outgrowth. Error bars represent standard error of mean. The x-axis reports the three different conditions, pLKO and RANBP2^{KD} cells (both shRNAs #1 and #3). Each experiment was performed in triplicates and both the scoring and the analysis were performed blinded. See also Figure S3.

Figure 4. Vinorelbine selectively kills *BRAF*-like CC cell lines

(A) Boxplot of $\log_{10}$ IC50 values for treatment of *BRAF(V600E)* and WT2 CC cell lines with vinorelbine (10 WT2 and 5 BRAF(V600E) cells), vinblastine (10 WT2 and 4 BRAF(V600E) cells), docetaxel (10 WT2 and 5 BRAF(V600E) cells) and paclitaxel (6 WT2 and 2

BRAF(V600E) cells) extracted from the Genomics of Drug Sensitivity in Cancer project. Shown are $\log_{10}$ of IC50 values (μM).

(B) Boxplot of $\log_{10}$ IC50 values for treatment of 11 BRAF-like CC cell lines (Vaco432, WiDr, HT29, RKO, SNU-C5, KM20, OXCO-1, SW1417, SKCO-1, HCT116, LoVo) and 11 non-*BRAF*-like CC cell lines (LIM1215, Difi, Caco2, HCA-7, HDC54, LIM1863, HCT15, SW480, SW1116, SNU1033, HCA-46) with vinorelbine, vinblastine and paclitaxel. Cells were treated with vinorelbine, vinblastine or paclitaxel for 72 hours. Shown are $\log_{10}$ of IC50 values (nM). See Table S4

(C-F) WT2 non-*BRAF*-like, *BRAF(V600E)*, *KRAS* mutant non-*BRAF*-like and *KRAS* mutant *BRAF*-like CC cells were seeded at low confluence and treated with increasing concentrations of vinorelbine twice a week. Viability was assessed by colony formation assay. Cells were fixed, stained and photographed after 10 days of culture.

(G-H) Vinorelbine induces mitotic arrest followed by apoptosis in *BRAF*-like CC cells. H2B-YFP WT2 CC cells (LIM1215, Caco2, HCT15) and H2B-YFP *BRAF*-like CC cells (WiDr, RKO, HCT116) were treated with vinorelbine (10nM) and filmed by time lapse microscopy over a period of 24hrs (G) and 72hrs (H) Per each CC cell lines, quantification of the main phenotypes occurring upon 24 hours (G) or 72 hours (H) of vinorelbine treatment are reported. A minimum of 90 cells per conditions were counted. See also Figure S4.

Figure 5. Vinorelbine suppresses *BRAF*-like tumor growth *in vivo*.

(A-E) Vinorelbine can selectively suppress *BRAF*-like tumor growth in xenograft models.

VACO432 cells (*BRAF*-like) (A), HCT116 cells (BRAF-like) (B), SW480 cells (non-*BRAF*-like) (C), HCT15 (non-BRAF-like) (D) and RKO cells (*BRAF*-like) (E), were grown as tumor xenografts in CD-1 nude mice. After tumor establishment (200-250 mm^3), mice were treated with either vehicle or vinorelbine (10 mg/kg i.v.) for the time indicated on each graph. Mean tumor volumes +/- standard error of the mean (n=5-6 mice per group). Arrow indicates initiation of treatment. See also Figure S5.

(F-I) Vinorelbine can selectively suppress BRAF-like tumor growth in orthotopic-implanted models.

Caco2 (non-*BRAF*-like) (F), HCT15 (non-*BRAF*-like) (G), WiDr (*BRAF*-like) (H) and HT116 (*BRAF*-like) (I) CC cell lines were used for orthotopic implantation experiment in nude mice. Animals were treated with vehicle or vinorelbine (2.5 mg kg^{-1}) for 2 weeks. Mean tumor volumes or weights ± standard error of the mean are shown (*n*=7-9 mice per group).

Figure 6. Vinca alkaloids show significant activity in BRAF-like CC tumors.

(A-B) Vulnerability to vinorelbine of CC cells implanted into liver revealed by intravital microscopy. (A) Cartoon showing the experimental set-up. Caco2 (non-*BRAF*-like) or SNU-C5 (*BRAF*-like) CC cells labeled with H2B-Dendra2 were injected into the liver of NSG mice. Upon tumor formation an abdominal imaging window was implanted on the liver of the recipient mice. The mice were intravitally imaged for three consecutive days, tracing back the same imaging areas each time point. Vehicle (PBS) or vinorelbine was administered immediately after the first imaging session.

Representative examples of mitotic figures and cell fragments upon cell death collected with intravital microscopy. Scale bar, 10 μm.

(B) Intravital imaging of Caco2 (non-*BRAF*-like) and Snu-c5 (*BRAF*-like) liver tumor before, 24hrs and 48hrs after vinorelbine administration. Red dashed lines highlight cells undergoing mitosis. White dashed lines indicate cell fragments. Scale bar, 50 μm. See also Figure S6

(C) BRAFV600E mutation is a discriminant of sensitivity to DM4 toxin in colon cancer PDX models.

Graphical representation of the percentage of *BRAF*(V600E) PDX models within DM4 toxin resistant and sensitive CC PDX models. The y-axis indicates the percentage of BRAFV600E mutant tumors within the two groups. The x-axis indicates the two groups, resistant and sensitive to DM4 toxin. See also Figure S6 and Table S5

(D) Complete remission of a BRAF-like metastatic CC patient upon vinblastine treatment

On the y-axis the BRAF FFPE scores of 207 FFPE samples, scores are sorted. Black indicates predicted by signature as non BRAF-Like, green indicates predicted by signature as BRAF-Like, red indicate sample T14-61892, red line indicates current cutoff for FFPE samples. See also Figure S6 and Table S5.

Figure 1

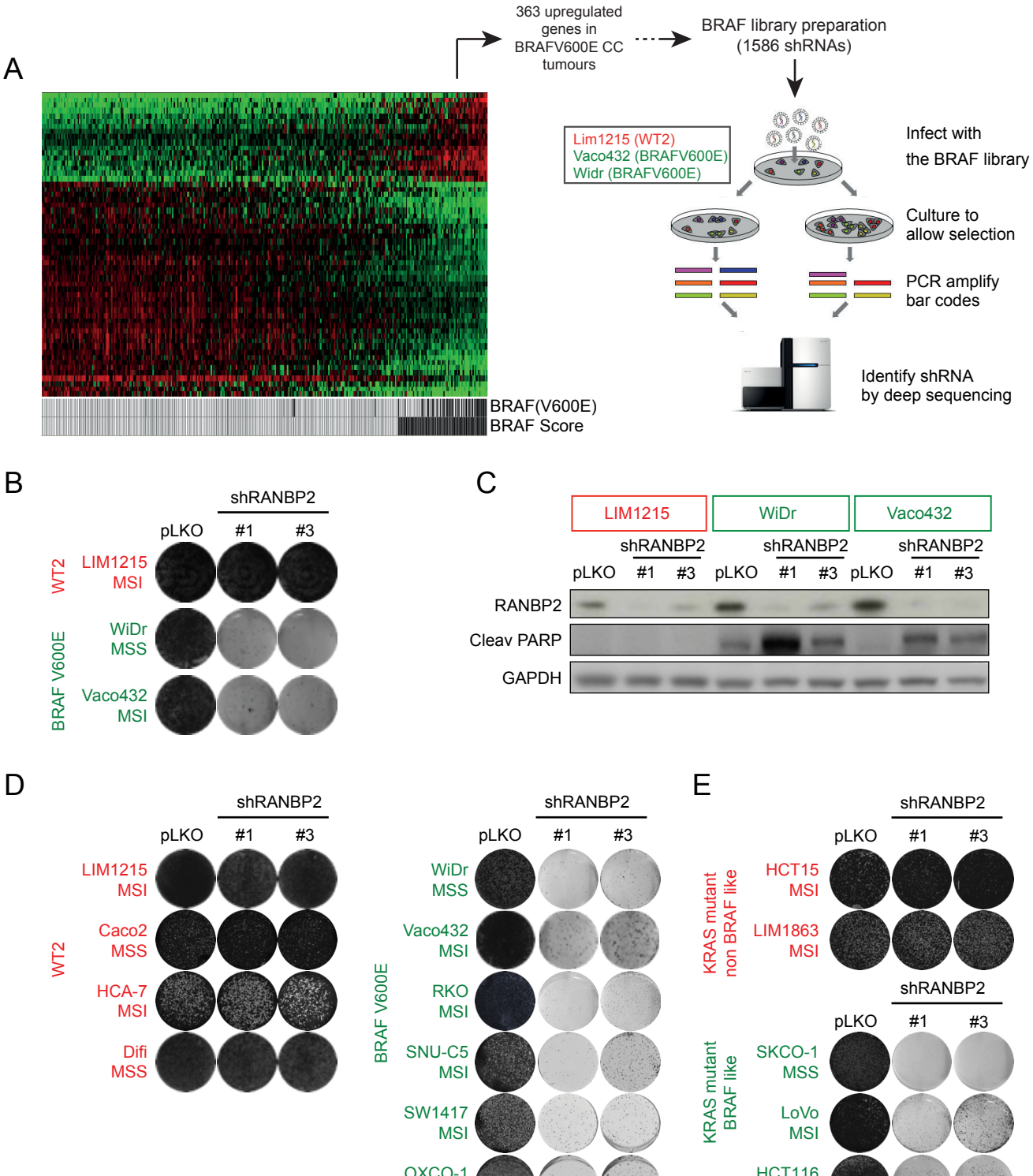
A
363 upregulated genes in BRAFV600E CC tumours
BRAF library preparation (1586 shRNAs)
Lim1215 (WT2)
Vaco432 (BRAFV600E)
Widr (BRAFV600E)
Infect with the BRAF library
Culture to allow selection
PCR amplify bar codes
Identify shRNA by deep sequencing
BRAF(V600E)
BRAF Score
B
shRANBP2
pLKO
#1
#3
WT2
LIM1215 MSI
BRAF V600E
WiDr MSS
Vaco432 MSI
C
LIM1215
WiDr
Vaco432
shRANBP2
pLKO
#1
#3
RANBP2
Cleav PARP
GAPDH
D
shRANBP2
pLKO
#1
#3
WT2
LIM1215 MSI
Caco2 MSS
HCA-7 MSI
Difi MSS
BRAF V600E
WiDr MSS
Vaco432 MSI
RKO MSI
SNU-C5 MSI
SW1417 MSI
OXCO-1 MSS
E
shRANBP2
pLKO
#1
#3
KRAS mutant non BRAF like
HCT15 MSI
LIM1863 MSI
KRAS mutant BRAF like
SKCO-1 MSS
LoVo MSI
HCT116 MSI

Figure 2

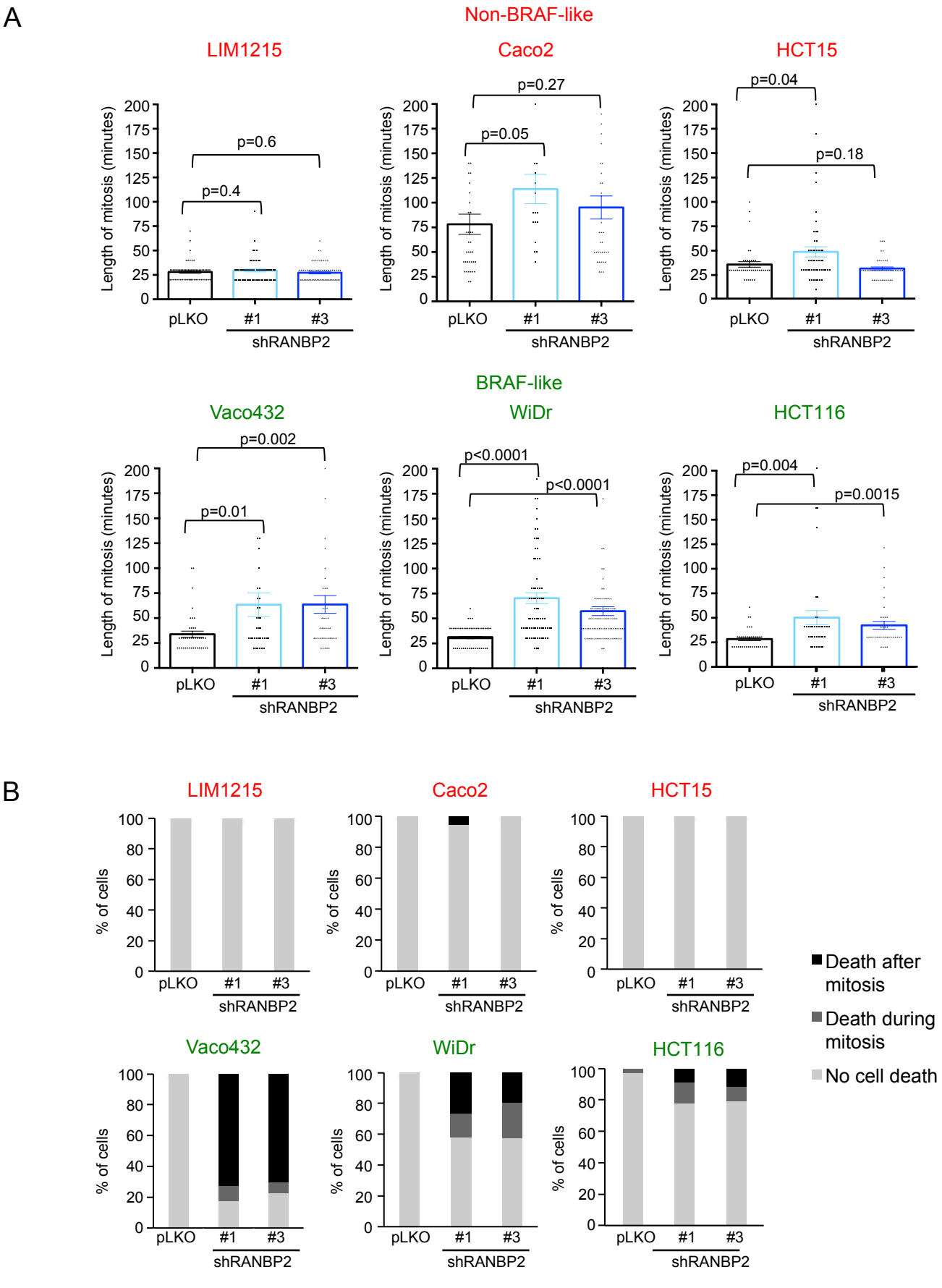
A
Non-BRAF-like
LIM1215
Caco2
HCT15
Length of mitosis (minutes)
p=0.6
p=0.4
p=0.27
p=0.05
p=0.04
p=0.18
pLKO
#1
#3
shRANBP2
BRAF-like
Vaco432
WiDr
HCT116
p=0.002
p=0.01
p<0.0001
p<0.0001
p=0.004
p=0.0015
B
% of cells
Death after mitosis
Death during mitosis
No cell death

Figure 3

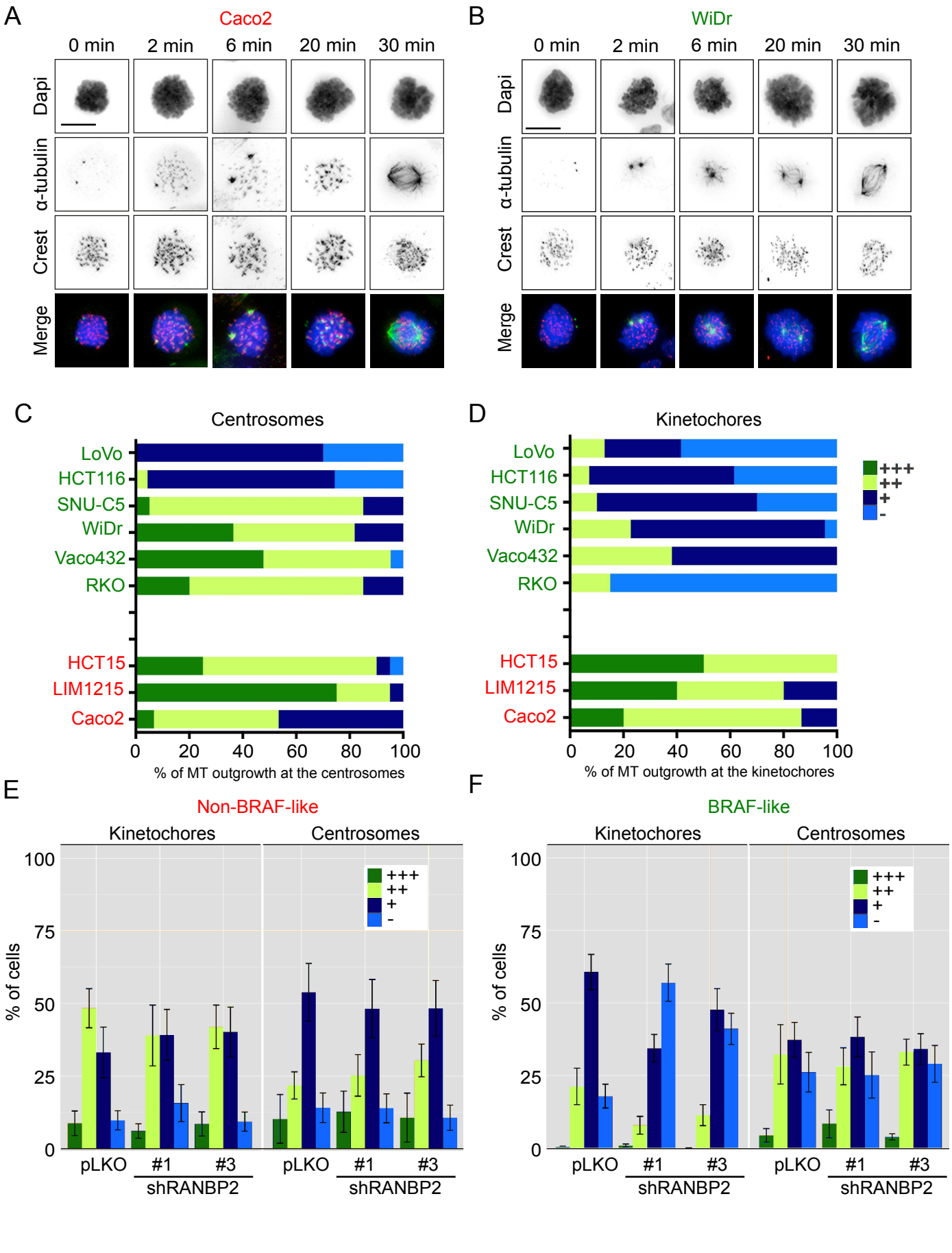
A
Caco2
0 min
2 min
6 min
20 min
30 min
Dapi
α-tubulin
Crest
Merge
B
WiDr
0 min
2 min
6 min
20 min
30 min
Dapi
α-tubulin
Crest
Merge
C
Centrosomes
LoVo
HCT116
SNU-C5
WiDr
Vaco432
RKO
HCT15
LIM1215
Caco2
0
20
40
60
80
100
% of MT outgrowth at the centrosomes
D
Kinetochores
LoVo
HCT116
SNU-C5
WiDr
Vaco432
RKO
HCT15
LIM1215
Caco2
+++
++
+
-
0
20
40
60
80
100
% of MT outgrowth at the kinetochores
E
Non-BRAF-like
Kinetochores
Centrosomes
100
75
50
25
0
% of cells
+++
++
+
-
pLKO
#1
#3
shRANBP2
F
BRAF-like
Kinetochores
Centrosomes
100
75
50
25
0
% of cells
+++
++
+
-
pLKO
#1
#3
shRANBP2

Figure 4

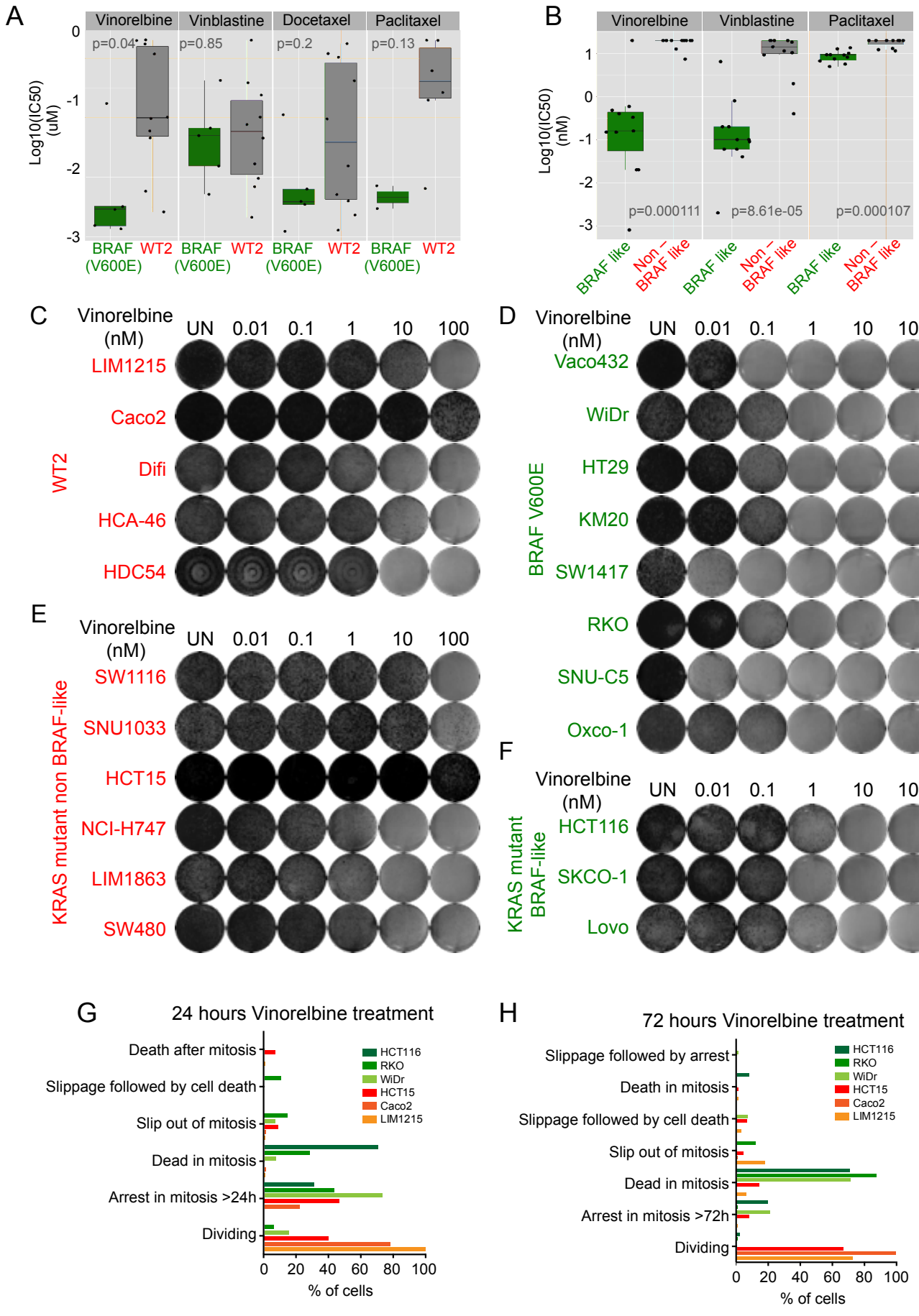
A
Vinorelbine
Vinblastine
Docetaxel
Paclitaxel
p=0.04
p=0.85
p=0.2
p=0.13
Log10(IC50) (uM)
BRAF (V600E)
WT2
B
Vinorelbine
Vinblastine
Paclitaxel
Log10(IC50) (nM)
p=0.000111
p=8.61e-05
p=0.000107
BRAF like
Non – BRAF like
C
Vinorelbine (nM)
UN 0.01 0.1 1 10 100
WT2
LIM1215
Caco2
Difi
HCA-46
HDC54
D
BRAF V600E
Vaco432
WiDr
HT29
KM20
SW1417
RKO
SNU-C5
Oxco-1
E
KRAS mutant non BRAF-like
SW1116
SNU1033
HCT15
NCI-H747
LIM1863
SW480
F
KRAS mutant BRAF-like
HCT116
SKCO-1
Lovo
G
24 hours Vinorelbine treatment
Death after mitosis
Slippage followed by cell death
Slip out of mitosis
Dead in mitosis
Arrest in mitosis >24h
Dividing
HCT116
RKO
WiDr
HCT15
Caco2
LIM1215
% of cells
H
72 hours Vinorelbine treatment
Slippage followed by arrest
Death in mitosis
Slippage followed by cell death
Slip out of mitosis
Dead in mitosis
Arrest in mitosis >72h
Dividing
% of cells

Figure 5

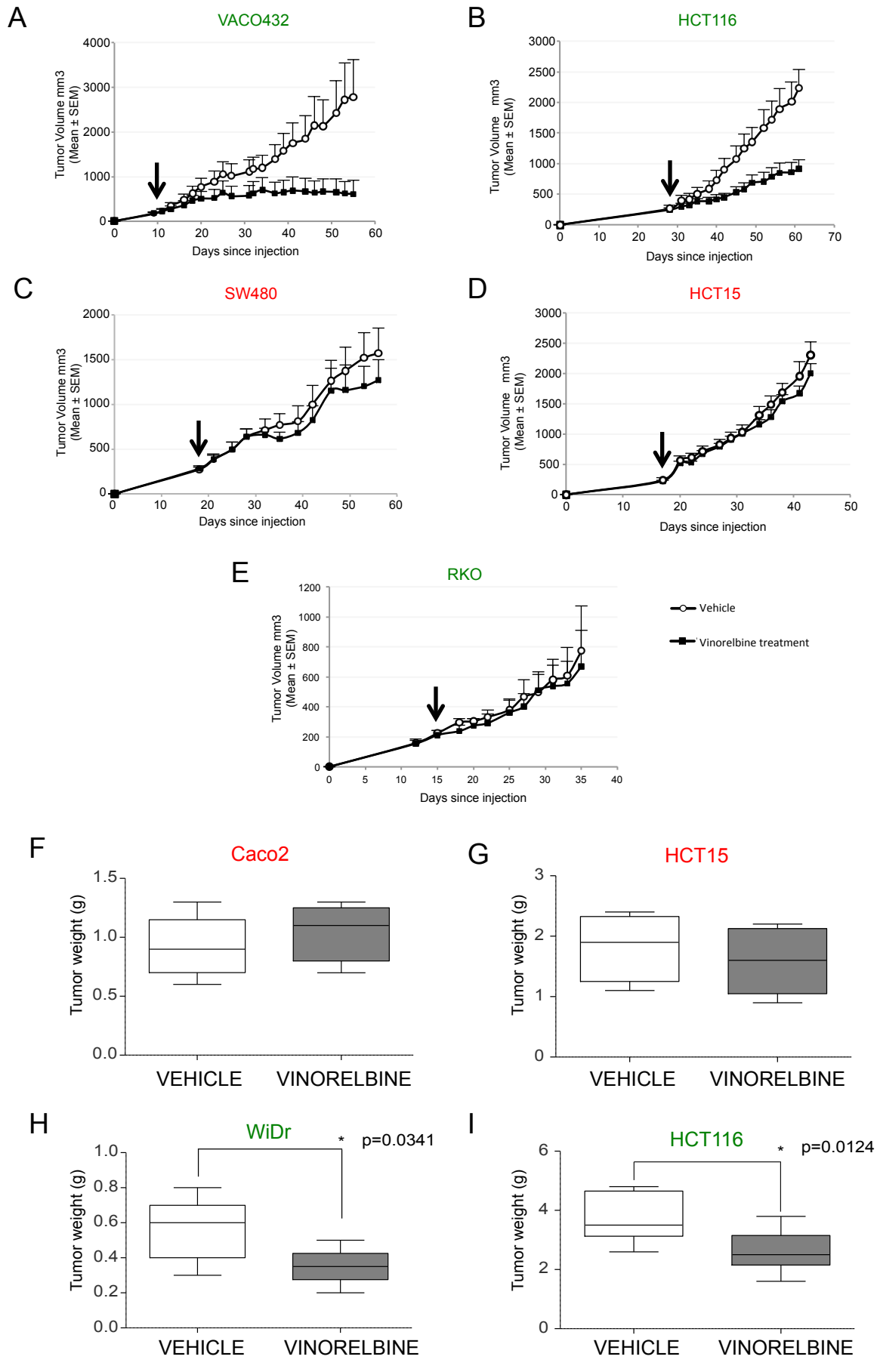
A
VACO432
Tumor Volume mm3 (Mean ± SEM)
Days since injection
B
HCT116
Tumor Volume mm3 (Mean ± SEM)
Days since injection
C
SW480
Tumor Volume mm3 (Mean ± SEM)
Days since injection
D
HCT15
Tumor Volume mm3 (Mean ± SEM)
Days since injection
E
RKO
Tumor Volume mm3 (Mean ± SEM)
Days since injection
Vehicle
Vinorelbine treatment
F
Caco2
Tumor weight (g)
VEHICLE
VINORELBINE
G
HCT15
Tumor weight (g)
VEHICLE
VINORELBINE
H
WiDr
Tumor weight (g)
*
p=0.0341
VEHICLE
VINORELBINE
I
HCT116
Tumor weight (g)
*
p=0.0124
VEHICLE
VINORELBINE

Figure 6

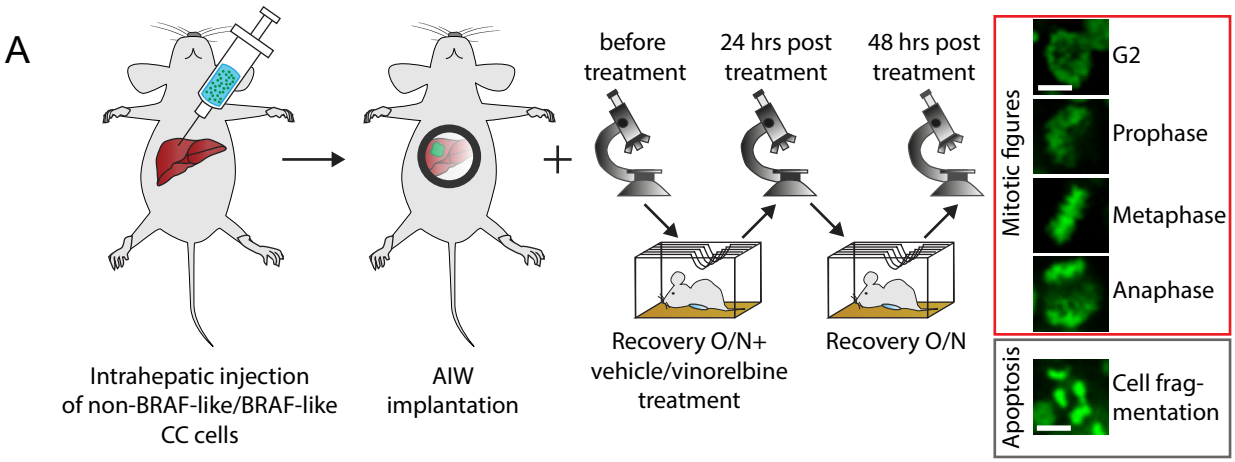
A
Intrahepatic injection of non-BRAF-like/BRAF-like CC cells
AIW implantation
before treatment
24 hrs post treatment
48 hrs post treatment
Recovery O/N+ vehicle/vinorelbine treatment
Recovery O/N
Mitotic figures
G2
Prophase
Metaphase
Anaphase
Apoptosis
Cell frag-mentation

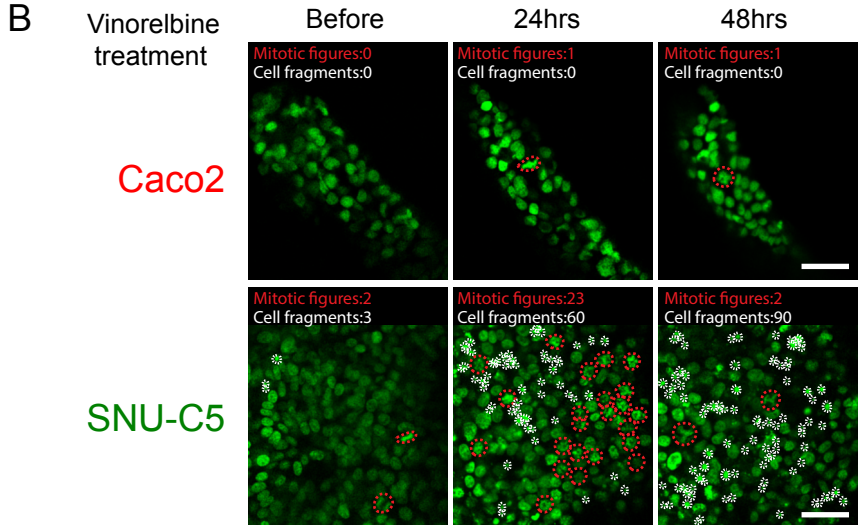
B
Vinorelbine treatment
Before
24hrs
48hrs
Caco2
Mitotic figures:0
Cell fragments:0
Mitotic figures:1
Cell fragments:0
Mitotic figures:1
Cell fragments:0
SNU-C5
Mitotic figures:2
Cell fragments:3
Mitotic figures:23
Cell fragments:60
Mitotic figures:2
Cell fragments:90

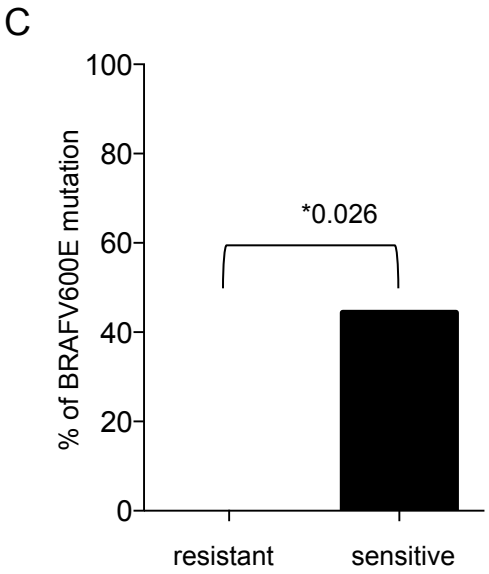
C
% of BRAFV600E mutation
100
80
60
40
20
0
*0.026
resistant
sensitive

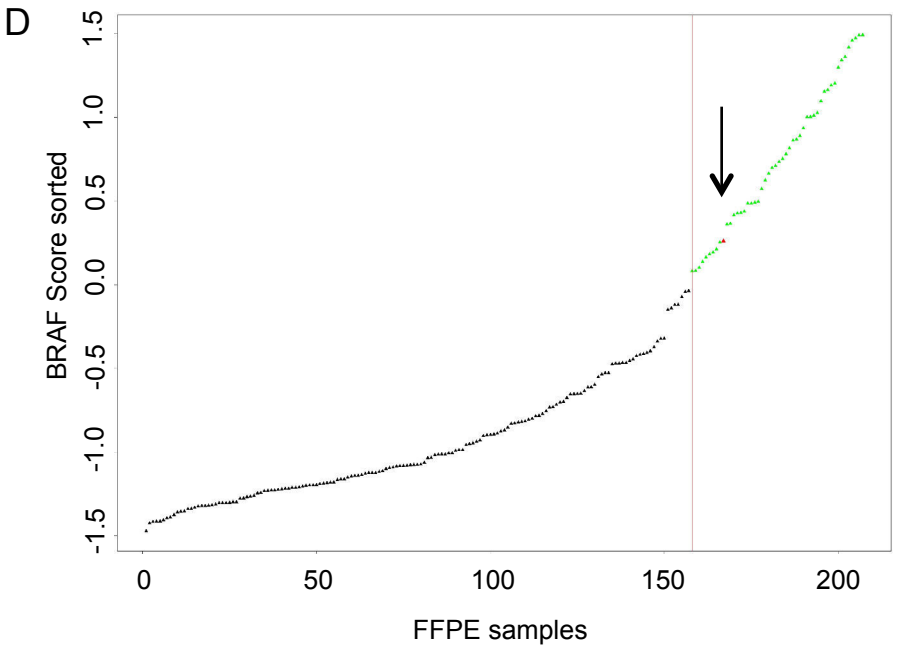
D
BRAF Score sorted
1.5
1.0
0.5
0.0
-0.5
-1.0
-1.5
0
50
100
150
200
FFPE samples

Supplemental Experimental Procedures

Reagents and Antibody Reagents

Vinorelbine, Paclitaxel and Vinblastine were obtained from the hospital pharmacy at The Netherlands Cancer Institute. Nocodazole was purchased from Sigma and was used at 500 ng/ml. PLX4032 and AZD6244 were purchased from Selleck Chemicals. TRC human genome-wide shRNA collection (TRC-Hs1.0) was purchased from Open Biosystems (Huntsville AL, USA). Further information is available at http://www.broad.mit.edu/genome_bio/trc/rnai.html. Recombinant human TGF-β1 (240-B) was purchased from R&D Systems.

Antibodies against RANBP2 (D-4, sc-74518), GAPDH (V-18, sc-20357), Cyclin B1 (GNS1, sc-245) were from Santa Cruz. Antibodies against Cleaved PARP (Asp 214, D64E10, XP, 5625S), total SMAD2 (3103), and pSMAD2 (3101) were from Cell Signaling.

Pooled shRNA ''Dropout'' Screen with the BRAF library

A total of 1586 short hairpin RNAs was picked from the TRC human genome wide shRNA collection (TRC-Hs1.0) to target the 363 genes composing the BRAF library. The BRAF library consists of four plasmids pools that were used to generate lentiviral supernatants as described at http://www.broadinstitute.org/rnai/ public/resources/protocols.

The *BRAF* library lentiviral supernatants were used to infect two *BRAF(V600E)* mutant CC cell lines (Vaco432 and WiDr) and one WT2 CC cell line (LIM1215). For each cell line, we performed four separate infections using the four lentiviral pools with a multiplicity of infection (MOI) <0.5. After puromycin selection, the infected cells were pooled and plated in 15 cm dishes at low density (350,000cells/dish). The number of cells plated for each cell line was sufficient to represent the BRAF library with a 400 times coverage per each shRNA present in the BRAF library. The cells were cultured for an additional 13 days. After this, cells were collected, genomic DNA was isolated (Brummelkamp et al., 2006) and used for recovery of the shRNA inserts by PCR with the primers PCR1 and PCR2 (see table) using the following conditions: (1) 98−C, 30 s; (2) 98−C, 10 s; (3) 60−C, 20 s; (4) 72−C, 1 min; (5) to step 2, 15 cycles; (6) 72−C, 5 min; (7) 4−C. Indexes and adaptors for deep sequencing (Illumina) were incorporated into PCR primers. 2.5 ul of the first PCR was used as input for for the 2nd PCR reaction using the primers PCR2 forward and PCR2 reverse (see table). PCR products were purified using QIAGEN PCR purification Kit according to the manufacturer manual. The amount of DNA was quantified using the BioAnalyzer and samples were combined at the same molar ratio. The shRNA sequences were extracted from the sequencing reads and aligned to TRC library. The matched reads were counted and the read counts were used for analysis. For the analysis, the read counts of the two independent infections in LIM1215 were treated as replicate one and two for the wild type condition. The read counts for the Vaco432 and WiDr cell lines were used as respectively, replicate one and replicate two for the BRAF-like condition. The statistical analysis was done using DESeq version 1.8.3 using the default settings for "pooled". The results of the DESeq analysis were used to calculate the ratio between WT and BRAF-like for each individual shRNA. .

Primers used are as follows**:**

PCR1 forward primers:

Lim1215 Time0(To) replicate#1	ACACTCTTTCCCTACACGACGCTCTTCCGATCTCGTGATCTTGTGGAAAGGACGAAAC CCGG
Lim1215 Time0(To) replicate#2	ACACTCTTTCCCTACACGACGCTCTTCCGATCTACATCGCTTGTGGAAAGGACGAA ACACCGG
Lim1215 7days(T7) replicate#1	ACACTCTTTCCCTACACGACGCTCTTCCGATCTGCCTAACTTGTGGAAAGGACGAA ACACCGG
Lim1215 7days(T7) replicate#2	ACACTCTTTCCCTACACGACGCTCTTCCGATCTTGGTCACTTGTGGAAAGGACGAAA CACCGG

Lim1215 13days(T13) replicate#1	ACACTCTTTCCCTACACGACGCTCTTCCGATCTCACTGTCTTGTGGAAAGGACGAAACACCGG
Lim1215 13days(T13) replicate#2	ACACTCTTTCCCTACACGACGCTCTTCCGATCTATTGGCCTTGTGGAAAGGACGAAACACCGG
Lim1215 II Time0(To) replicate#1	ACACTCTTTCCCTACACGACGCTCTTCCGATCTTTTCACCTTGTGGAAAGGACGAAACACCGG
Lim1215 II Time0(To) replicate#2	ACACTCTTTCCCTACACGACGCTCTTCCGATCTGGCCACCTTGTGGAAAGGACGAAACACCGG
Lim1215 II Time7(T7) replicate#1	ACACTCTTTCCCTACACGACGCTCTTCCGATCTCGAAACCTTGTGGAAAGGACGAAACACCGG
Lim1215 II Time7(T7) replicate#2	ACACTCTTTCCCTACACGACGCTCTTCCGATCTCGTACGCTTGTGGAAAGGACGAAACACCGG
Lim1215 II Time13(T13) replicate#1	ACACTCTTTCCCTACACGACGCTCTTCCGATCTCCACTCCTTGTGGAAAGGACGAAACACCGG
Lim1215 II Time13(T13) replicate#2	ACACTCTTTCCCTACACGACGCTCTTCCGATCTGCTACCCTTGTGGAAAGGACGAAACACCGG
WiDr Time0(To) replicate#1	ACACTCTTTCCCTACACGACGCTCTTCCGATCTGATCTGCTTGTGGAAAGGACGAAACACCGG
WiDr Time0(To) replicate#2	ACACTCTTTCCCTACACGACGCTCTTCCGATCTTCAAGTCTTGTGGAAAGGACGAAACACCGG
WiDr 7days(T7) replicate#1	ACACTCTTTCCCTACACGACGCTCTTCCGATCTCTGATCCTTGTGGAAAGGACGAAACACCGG
WiDr 7days(T7) replicate#2	ACACTCTTTCCCTACACGACGCTCTTCCGATCTAAGCTACTTGTGGAAAGGACGAAACACCGG
WiDr 13days(T13) replicate#1	ACACTCTTTCCCTACACGACGCTCTTCCGATCTGTAGCCCTTGTGGAAAGGACGAAACACCGG
WiDr 13days(T13) replicate#2	ACACTCTTTCCCTACACGACGCTCTTCCGATCTTACAAGCTTGTGGAAAGGACGAAACACCGG
Vaco432 Time0(To) replicate#1	ACACTCTTTCCCTACACGACGCTCTTCCGATCTTTGACTCTTGTGGAAAGGACGAAACACCGG

Vaco432 Time0(To) replicate#2	ACACTCTTTCCCTACACGACGCTCTTCCGATCTGGAACTCTTGTGGAAAGGACGAA ACACCGG
Vaco432 7days(T7) replicate#1	ACACTCTTTCCCTACACGACGCTCTTCCGATCTTGACATCTTGTGGAAAGGACGAAA CACCGG
Vaco432 7days(T7) replicate#2	ACACTCTTTCCCTACACGACGCTCTTCCGATCTGGACGGCTTGTGGAAAGGACGAA ACACCGG
Vaco432 13days(T13) replicate#1	ACACTCTTTCCCTACACGACGCTCTTCCGATCTCTCTACCTTGTGGAAAGGACGAAA CACCGG
Vaco432 13days(T13) replicate#2	ACACTCTTTCCCTACACGACGCTCTTCCGATCTGCGGACCTTGTGGAAAGGACGAA ACACCGG
P7_pLKO1_r (PCR1 reverse primer)	CAAGCAGAAGACGGCATACGAGATTTCTTTCCCCTGCACTGTACCC
P5_IlluSeq (PCR2 Forward primer)	AATGATACGGCGACCACCGAGATCTACACTCTTTCCCTACACGACGCTCTTCCGATC T
P7 (PCR2 Forward primer)	CAAGCAGAAGACGGCATACGAGAT

Cell Culture and Viral Transduction

HDC-54 colon cancer (CC) cell line was cultured in DMEM/F12 with 10% heat-inactivated fetal bovine serum, penicillin and streptomycin at 5% CO_2. All the other colon cancer cell lines were cultured in RPMI with 10% heat-inactivated fetal bovine serum, penicillin and streptomycin at 5% CO_2. HEK293T Phoenix cells were cultured in DMEM with 10% heat-inactivated fetal bovine serum penicillin and streptomycin at 5% CO_2. HEK293T cells were used as producers of lentiviral supernatants as described at http://www.broadinstitute.org/rnai/public/resources/protocols. Both the calcium phosphate method and the PEI (Polyethylenimine 25kD linear) reagent were used for the transfection of 293T cells. PEI reagent was from Polysciences (cat# 23966-2) and used according to the manufacturer' instructions. Infected cells were selected for successful lentivirus integration using 2 mg/mL of puromycin (Caco2 and HCT15 cell lines were selected using 10mg/mL of puromycin; SKCO-1 cell line was selected using 1mg/mL of puromycin).

Constructs

All lentiviral shRNA vectors were retrieved from the arrayed TRC human genome-wide shRNA collection (TRC-Hs1.0). Additional information about the shRNA vectors can be found at http://www.broadinstitute.org/rnai/public/clone/search using the TRCN number. The following lentiviral shRNA vectors were used: sh*RANBP2*#0, TRCN0000003450; sh*RANBP2*#1, TRCN0000003451; sh*RANBP2*#2, TRCN0000003452; sh*RANBP2*#3, TRCN0000003453; sh*RANBP2*#4, TRCN0000003454. As control we used a scrambled shRNA sequence with the same nucleotide composition as the RANBP2 KD TRCN0000003453. For time lapse experiments, CC cell lines were either transduced with histone H2B-GFP lentiviral construct (LV-GFP, Addgene plasmid#25999) or the histone H2B-YFP (Kanda et al., 1998).

Time lapse live imaging

To allow visualization of chromosomes, cells were transduced with either a histone H2B-GFP (LV-GFP, Addgene plasmid#25999) or a histone H2B-YFP. Cells were then plated 24 hours before starting the microscope acquisition and, where described, vinorelbine 10nM was added in the medium 1 hour before starting the movie. For the vinorelbine experiment cells were filmed over 24 hours and 72 hours and pictures were taken either every 3 minutes or every 10 minutes. For the RANBP2 KD experiment, cells were filmed over 72 hours and pictures were taken every 10 minutes. Cells were tracked using a Zeiss AxioObserver.Z1 microscope setup with a temperature and CO_2 controlled chamber equipped with a LD condenser 0.55 and a 20x / 0.40 LD Achroplan Ph2 phase contrast objective. GFP Zeiss Filter Set-38HE and YFP Zeiss Filter Set 46HE were used to acquire fluorescence. Images were taken using a Hamamatsu ORCA R2 Black and White CCD-camera and processed by using ZEN2012 software. For each condition filmed, 8 different fields were selected and followed for 72 hours. In each field we randomly choose and followed cells entering in mitosis (nuclear envelope breakdown, NEBD, was used as indicator of mitotic division onset).

Incucyte Cell live imaging

CC cells were plated in a 384 well plate (500, 1000 and 2000 cells per well) and cultured in the IncuCyte for 10 days. Plate density was measured every four hours and related to the average signal on the first day. Doubling time analysis was performed by exponential growth equation (GraphPad Software – Prism 6). The data of non BRAF-like cells were grouped together as well as the data of the BRAF like cells. Two groups were the compared by using a Mann-Whitney test.

qRT-PCR

qRT-PCR assays were carried out to measure mRNA levels of genes using 7500 Fast Real-Time PCR System (Applied Biosystems) as described (Kortlever RM et al, 2006). Relative mRNA levels of each gene shown were normalized to the expression of the housekeeping gene *GAPDH*. The sequences of the primers for assays using SYBR Green master mix (Roche) are as follows: *GAPDH*_Forward, AAGGTGAAGGTCGGAGTCAA; *GAPDH*_Reverse, AATGAAGGGGTCATTGATGG; *RANBP2*_Forward ACAGCTTTGCAAAATAGAATCC; *RANBP2*_Reverse, CTGACGTGGAGCGGTACAT.

Immunofluorescence

Cells were grown either on a 24-mm or a 10-mm glass coverslips. After 24 hours after seeding, cells were treated with 500mg/mL nocodazole for 3 hours after which cells were carefully washed with medium for 4 times. At the corresponding time points, cells were fixed with 4% formaldehyde / 0.5% triton X-100 for 20 minutes. Cells were then washed 3 times with PBS 1X / 0.2% Tween. α-tubulin antibody (Sigma) was used at 1:10:000, ACA antibody (Cortex Biochem) was used at 1:2000. Primary antibodies were diluted in PBS 1X / 0.2% Tween and incubated overnight at 4 degrees. The day after, the coverslips were washed 3 times with PBS 1X / Tween 0.2% and incubated for 2 hours at room temperature with the following secondary antibodies (1:500 dilution): Alexa Fluor 488 REF A11029, Alexa Fluor 568 REF A21090, Alexa Fluor 647 REF A21445. Secondary antibodies were diluted in PBS 1X / Tween 0.2% together with DAPI. Secondary antibodies were from Life Technologies. After 2 hours incubation, coverslips were washed 3 times with PBS 1X / 0.2% Tween and mounted using Vectashield H-1000 (Vector laboratories, Inc Burlingame CA 94010). Images were acquired on a Deltavision Elite microscope (Applied Precision), taking 200-nm z-stacks using a PlanApo N 60×/NA 1.42 objective (Olympus) and a Coolsnap HQ2 camera (Photometrics). Figures were generated by maximum intensity projections of entire cells using Softworx (Applied Precision). Brightness and contrast were adjusted with Photoshop 6.0 (Adobe). Changes in microtubule outgrowth were assessed by paired t-tests as implemented in the R statistical programming environment pooling the three replicates of both BRAF mutant-like cell lines and both non BRAF mutant-like cell lines. We individually compared each category (“-“, “+”,”++”, “+++”) between control cells (pLKO) and either of the hairpins (#1 or #3). P-values were then corrected for multiple testing using the Benjamini-Hochberg false discovery rate (FDR) procedure.

Short-term viability assay

Cells were seeded into 96-well plate (7000 cells/well) and twenty-four hours after seeding, cells were treated with vinorelbine, vinblastine (final drug concentrations ranging from 0.0001nM to 100nM) or paclitaxel (final drug concentration ranging from 0.03125 to 20 nM) After 72 hours of incubation, cell viability was measured using crystal violet staining absorbance. Relative survival in the presence of drugs was normalized to the untreated controls after background subtraction. IC50 was calculated fitting a dose response curve by using GraphPad Software – Prism 6. For the experiment reported in Supplementary Fig.5 RKO cells were first exposed to recombinant human TGF-β1 (200pM) for 4, 7 and 10 days and then seeded into 96-well plate in presence of TGF-β1 (7000 cells/well; each condition in

triplicate). Twenty-four hours after seeding, cells were treated with vinorelbine (final drug concentrations ranging from 0.0001nM to 100nM) in combination with recombinant human TGF-β1 (200 pM). After 72 hours of incubation, cell viability was measured using crystal violet staining absorbance. RKO parental cells not exposed to TGF-β1 were used as comparison arm. Relative survival in the presence of drugs was normalized to the untreated controls after background subtraction. The curves represent the median of three independent experiments with relative SD for each concentration.

Xenografts

Vaco432, HCT116, SW480, HCT15 and RKO CC cells were injected (7-8X10^6 cells per mouse) subcutaneously in the right flank of 8-week-old immunodeficient CD1 nude female mice (from Charles River Laboratory). Tumor volume was monitored twice a week by digital caliper and quantified by the modified ellipsoidal formula (tumor volume = 1/2(length × width^2). Mice were randomized (5-6 mice per group) when they reached a volume of approximately 200 mm^3 and treated for 3-6 weeks, as described in figure legends. Vinorelbine (10mg/Kg) was administered once a week by intravenous injection. All animal procedures were approved by the Ethical Commission of the Fondazione Piemontese per la Ricerca sul Cancro ONLUS and by the Italian Ministry of Health and they were performed in accordance with institutional guidelines.

Orthotopic models

Drugs and cell lines

Vinorelbine was obtained from the Pharmacy of Catalan Institut of Oncology (ICO), L'Hospitalet de Llobregat , Barcelona. WiDr cell line were a kind gift from Dr. L. Espinosa (Institut Municipal d'Investigacions Mèdiques (IMIM)-Hospital del Mar, Parc de Recerca Biomèdica de Barcelona (PRBB), Barcelona, Spain) and Caco2, HCT116 and HCT15 were from Dr. Bernards (Division of Molecular Carcinogenesis - NKI/AVL - Amsterdam, the Netherlands). Cell cultures were grown in vitro at 37 ºC in a humidified atmosphere of 5% CO2 in Dulbecco's modified Eagle's medium (DMEM) supplemented with 10% fetal bovine serum and antibiotics.

Drug response in orthotopically engrafted cell-line derived tumors

Athymic *nu/nu* mice (Harlam, France), aged 4-5 weeks, were used for tumor xenografts. The animals were maintained in a sterile environment; their cages and bedding were sterilized by autoclaving and food were γ-ray sterilized. A panel of four colorectal tumor cell lines with different mutational *BRAF*/*KRAS* status were used for the generation of orthotopic engrafted tumors and drug response experiments: WiDr (*BRAF* (V600E)/*KRAS*(WT)/BRAF-like); Caco-2 (*BRAF* (WT)/*KRAS*(WT)/non BRAF-like), HCT116 *(BRAF* (WT)/*KRAS mut* BRAF-like) and HCT-15 *(BRAF* (WT)/*KRAS mut* non BRAF-like). All cell lines were cultured in DMEM medium supplemented with 10% fetal bovine serum at 37°C and 5% CO_2. For each cell line, 3.5 x 10^6 cells diluted 200 µl of PBS were mixed with 100 µl of Matrigel and were subcutaneously (s.c.) injected in anesthetized athymic (n=5 animals/cell line) *nu/nu* mice (Harlan) (*Pre-experiment*). Once the tumor had grown to 800-1000 mm^3, it was cut into 3-5x3-5 mm^3 pieces and maintained in DMEM supplemented medium with 10% fetal bovine serum and penicillin/streptomycin. Those viable fragments with macroscopically low or absent levels of necrotic areas were selected for orthotopic implantation (*Drug Response Experiment*). Briefly, nude mice were anesthetized by isoflurane inhalation and small fragments of 5 mm^3 were anchored to the *ceacum* surface with a Prolene 7.0 suture, as we described previously(Aytes et al., 2012; Melo et al., 2011). The abdominal incision was closed with surgery staples and mice were inspected twice a week. Mice were engrafted (n=20/each tumor) with WiDr, HCT116, HCT-15 and Caco-2 derived subcutaneous xenografts. When tumors reached a homogeneous palpable size they were randomly allocated into the treatments groups (n=7-9/group): i) Vehicle (saline); ii) Vinorelbine (2.5 mg/kg). To reduce the vinorelbine induced toxicity, it was administered intraperitoneally (i.p) every second day (days 0, 2, 4, 6, 8, 10 and 12) for two consecutive weeks. At day 15, mice were sacrificed, their colon + tumor dissected out, weighed, and the tumor volumes were estimated from two-dimensional caliper measurements using the equation V = (π/6) x L x W2, where V = volume (mm3), L = length (mm), and W = width (mm), and reported as volume mean ± SEM for each mouse group. Representative fragments were either frozen in nitrogen or fixed and then processed for paraffin embedding. Statistical significance among treatments was analyzed by Mann-Whitney and ANOVA tests for two o three comparisons, respectively. All animal experiments were approved by the IDIBELL Ethical Committee and performed in accordance with guidelines stated in The International Guiding Principles for Biomedical Research involving Animals, developed by the Council for International Organizations of Medical Sciences (CIOMS) in the Animal Core Facility of IDIBELL (AAALAC Unit 1155).

Intravital imaging

Cell culture

Caco2 (non-BRAF-like) Snu-c5 (BRAF-like) CC cells were infected with lentivirus carrying pLV.CMV.puro.H2BDendra. After infection cells were selected with 5µg/ml puromycin (Sigma).

Intravital microscopy

All intravital imaging experiments were approved by the animal ethical committee (DEC) of the Netherlands Academy of Sciences (KNAW), the Netherlands. Animals were kept at the Hubrecht animal facility in Utrecht, the Netherlands. To induce liver metastases, 300,000 CC cells were mixed in a 100µl solution containing Matrigel (Basement Membrane Matrix Growth Factor Reduced Phenol Red Free, Corning) and PBS (2.5:1) and injected into the liver of NOD scid gamma (NSG) mice. Two (for BRAF-like liver metastases) or three weeks (for non-BRAF-like liver metastases) after cell intrahepatic injection an abdominal imaging window was surgically implanted as described recently(Ritsma et al., 2012, 2013). The surgical procedures were performed under 2% isoflurane inhalation anesthesia and under aseptic conditions. Before surgery the mice were treated with a sub-cutaneous injection of buprenorphine (3mg per mouse, Temgesic, BDPharmaceutical System). After surgery, the mice were kept at 37°C until fully recovered. For every imaging session, mice were sedated using isoflurane inhalation anesthesia (~1.5% isoflurane/O2 mixture), and placed with their head in a facemask within a custom designed imaging box. The imaging box and microscope were kept at 36.5°C using a climate chamber. After the first imaging session the mice were treated intravenously with either a vehicle control (100µl of sterile PBS) or vinorelbine drug (10mg/ml). Between the imaging sessions, mice were let recover in their cage. Intravital images were acquired with an inverted Leica TCS SP5 AOBS two-photon microscope (Mannheim, Germany) with a chameleon Ti:Sapphire pumped Optical Parametric Oscillator (Coherent Inc. Santa Clare, CA, USA). The imaging areas were retraced in subsequent imaging sessions by storing the stage coordinates of the imaging areas, tracking photo-marked Dendra2 cells and by visual landmarks such as blood vessels as described in Ritsma et al. (Ritsma et al., 2014).

Patient –derived xenograft (PDX)

Patient-derived xenografts (PDX) have already been established and characterized (Julien et al., 2012).
Procedures involving animal were conducted in accordance with the conditions established by the European Community (2010/63/EU Directive) and approved by the Sanofi Animal Care and Use Committee.
Intrinsic sensitivity is defined as the sensitivity of a model to a drug independently of the expression of cell membrane targets. It was assessed by treating 20 CRC (PDX)-implanted mice with a high dose of an ADC made of an antibody specific for CD19, an antigen expressed in B-lymphocytes. The antibody is attached to DM4 through a cleavable N-succinimidyl-3-(2-pyridyldithio) butyrate (SPDB) linker. As CD19 antigen is not expressed in CRC PDX, the antitumor activity after treatment with a high dose of the ADC is non-specific i.e. cytotoxic DM4 released from the ADC and/or coming from antigen-independent internalization of the ADC.
Severe combined immunodeficient (SCID) female mice, 8- to 10-week-old, bred at Charles River France, were at least 18 g at the start of treatment and had free access to food and sterile water. Patient-derived colon xenografts (PDX) previously described (Julien et al., 2012) were engrafted as small fragments (50 mm3) on the flank of female SCID mice, tumors were allowed to grow to the desired volume range and the mice were then pooled and unselectively distributed based on tumor size on the day of first treatment to the treatment and control groups (6 to 8 mice per group).
Tumor volumes (in mm^3) based on the following formula, volume = length (mm) x $width^2$ (mm^2) / 2, were measured twice weekly and body weight recorded every day. Efficacy endpoints collected were the tumor volume changes from baseline summarized by the ratio of medians between treated and control groups ($\Delta T/\Delta C$) expressed in percentage, complete regressions (CR, regression below the palpable limit 14 mm^3), partial regressions (PR, regression of 50% of the initial tumor volume), and the percent median regression (% of volume decrease post-treatment compared with pre-treatment). Interpretation of the $\Delta T/\Delta C$ expressed in percentage was based on the following criteria: inactive when $\Delta T/\Delta C > 40\%$, marginally active when $25\% < \Delta T/\Delta C \leq 40\%$, active with obvious tumor growth delay when $10\% < \Delta T/\Delta C \leq 25\%$, active with tumor stasis when $0\% \leq \Delta T/\Delta C \leq 10\%$, and highly active with tumor regression when $\Delta T/\Delta C$ is lower than 0%

Sequencing of BRAF exon 15

Molecular characterization included gene sequencing of the major mutation hotspots in CRC was previously performed(Julien et al., 2012). In order to test for the BRAF V600E mutations (BRAF c.1799T>A), a direct Sanger was

performed. Briefly, after PCR amplification, purified PCR products were sequenced using Big Dye Terminator Kit V3.1 (Life Technologies) according to the manufacturer's recommendations. Sequencing reactions were then carried out on a 96-capillary 3730xl DNA Analyzer.

Patient's data

FFPE template and FFPE cutoff of BRAF 58-gene signature was calibrated on 206 samples (BRAF-mut n=23, WT n=183) that passed QC model. Samples were hybridized on Agilent DX2 full genome array (amid 32627) and normalized by using 461 colon tumor specific normalization genes. The formula used for calculation of BRAF 58-gene signature scores was following:

$$\text{BRAFm like score} = 3 \times (\text{pearscorr}(\text{sample}, \text{BRAFmut}) - \text{pearscorr}(\text{sample}, \text{Wildtype})) + \text{pearsoncorr}\left(\frac{\text{sample} - (\text{BRAFmut} + \text{wildtype})}{2}, \frac{\text{sample} - (\text{BRAFmut} + \text{wildtype})}{2}\right)$$

The performance on FFPE samples was estimated by Leave-One-Out-Cross-Validation and resulted in a sensitivity of 87% (20/23) and specificity of 83% (152/183).

Supplemental References

Aytes, A., Molleví, D.G., Martinez-Iniesta, M., Nadal, M., Vidal, A., Morales, A., Salazar, R., Capellà, G., and Villanueva, A. (2012). Stromal interaction molecule 2 (STIM2) is frequently overexpressed in colorectal tumors and confers a tumor cell growth suppressor phenotype. Mol. Carcinog. *51*, 746–753.

Brummelkamp, T.R., Fabius, A.W.M., Mullenders, J., Madiredjo, M., Velds, A., Kerkhoven, R.M., Bernards, R., and Beijersbergen, R.L. (2006). An shRNA barcode screen provides insight into cancer cell vulnerability to MDM2 inhibitors. Nat. Chem. Biol. *2*, 202–206.

Julien, S., Merino-trigo, A., Lacroix, L., and Cancer, H.C. (2012). Characterization of a Large Panel of Patient-Derived Tumor Xenografts Representing the Clinical Heterogeneity of Human Colorectal Cancer Characterization of a Large Panel of Patient-Derived Tumor Xenografts Representing the Clinical Heterogeneity of. *18*, 5314–5329.

Kanda, T., Sullivan, K.F., and Wahl, G.M. (1998). Histone-GFP fusion protein enables sensitive analysis of chromosome dynamics in living mammalian cells. Curr. Biol. *8*, 377–385.

Kortlever RM, Higgins PJ, B.R. (2006). Plasminogen activator inhibitor-1 is a critical downstream target of p53 in the induction of replicative senescence. NAt Cell Biol *8*, 877–884.

Melo, S., Villanueva, A., Moutinho, C., Davalos, V., Spizzo, R., Ivan, C., Rossi, S., Setien, F., Casanovas, O., Simo-Riudalbas, L., et al. (2011). Small molecule enoxacin is a cancer-specific growth inhibitor that acts by enhancing TAR RNA-binding protein 2-mediated microRNA processing. Proc. Natl. Acad. Sci. U. S. A. *108*, 4394–4399.

Ritsma, L., Ellenbroek, S.I.J., Zomer, A., Snippert, H.J., de Sauvage, F.J., Simons, B.D., Clevers, H., and van Rheenen, J. (2014). Intestinal crypt homeostasis revealed at single-stem-cell level by in vivo live imaging. Nature *507*, 362–365.

Figure S1 Validation of RANBP2 as Synthetically Lethal with BRAF (V600E) in CC, Related to Figure 1B, C, D, E.

(A) 5 different shRNAs against RANBP2 present in the BRAF library impair cell growth in *BRAF(V600E)* CC cell lines. Vaco432 and WiDr, *BRAF(V600E)* CC cell lines and LIM1215, WT2 CC cell line, were stably infected with all the 5 shRNAs targeting *RANBP2* present in the BRAF library. Viability was assessed by colony formation assay. The pLKO vector was used as negative control. Cells were fixed, stained and photographed after 10 days of culture.

(B) The level of *RANBP2* ^{KD} by each of the five shRNAs was measured by examining the *RANBP2* mRNA level by q-RT-PCR. Error bars denote SD.

(C) In all the CC cell lines used for the screen validation, the level of RANBP2 protein knockdown was measured by western blot.

(D) The toxicity of RANBP2 knockdown in *BRAF* -like CC cells is specific.

WT2 CC cells (LIM1215, HCA7, Caco2), *BRAF(V600E)* CC cells (WiDr, Vaco432, OXCO-1), *KRAS* mutant non-*BRAF*-like CC cells (HCT15, LIM1863) and *KRAS* mutant *BRAF*-like CC cells (SKCO-1, HCT116) were stably infected with a scramble shRNA vector, pLKO empty vector and with two independent shRNAs targeting *RANBP2* (sh*RANBP2* #1, sh*RANBP2* #3). Viability was assessed by colony formation assay and parental cell lines were included as uninfected control. Cells were fixed, stained and photographed after 10 days of culture.

Figure S2. RANBP2 KD Induces Several Mitotic Defects in BRAF-Like CC Cells, Related to Figure 2A

(A) In all the CC cell lines used for the time lapse experiment (see also Figure 2A), the level of RANBP2 protein knockdown was measured by western blot.

(B)RANBP2 knockdown induces a plethora of mitotic defects in *BRAF*-like CC cell lines.

H2B-GFP non *BRAF*-like CC cells (LIM1215, Caco2, HCT15) and H2B-GFP *BRAF*-like CC cells (Vaco432, WiDr, HCT116) were stably infected with 2 different shRNAs targeting *RANBP2* (shRANBP2#1, shRANBP2#3) and followed by time-lapse microscopy (see also Figure 2A and experimental procedures). For each CC cell lines pLKO was used as a control. The y-axis indicates percentage of the most recurrent mitotic abnormalities observed during the time-lapse experiments in all the CC cell lines analyzed.

Figure S3. RANBP2 KD Reduces the Microtubule (MT) Nucleation from kinetochores in BRAF-Like CC Cells, Related to Figure 3E, F

(A) For both the centrosomes (panel on the left) and the kinetochores (panel on the right) are reported representative IF images per each of the categories scored as no ("-"), weak ("+"), medium ("++") or strong ("+++") microtubule outgrowth. Images are referring to one of the experiment conducted on Caco2 CC cell line. Scale bars indicate 10 μm. Cells were stained for α tubulin to visualize MTs, CREST to visualize the kinetochores and DAPI to visualize the DNA. See supplemental experimental procedure for details.

(B) In all the CC cell lines used for the nocodazole washout experiment, the level of RANBP2 protein knockdown was measured by western blot. See also Figure 3E and 3F.

(C-D) Quantification of microtubule outgrowth from kinetochores or centrosomes in non-*BRAF*-like CC cell line, Caco2 (C) and HCT15 (D). The y-axis indicates percentage of cells showing no ("-"), weak ("+"), medium ("++") or strong ("+++") microtubule outgrowth. Error bars represent standard error of mean. On the x-axis the three different conditions, pLKO and *RANBP2*^{KD} cells (both shRNA #1 and #3). The graph shows averages of three independent experiments with at least 40 cells scored per condition. See also supplemental experimental procedures. No statistically significant differences between conditions.

(E-F) Quantification of microtubule outgrowth from kinetochores or centrosomes in *BRAF*-like CC cell line, WiDr (E) and HCT116 (F). The y-axis indicates percentage of cells showing no ("-"), weak ("+"), medium ("++") or strong ("+++") microtubule outgrowth. Error bars represent standard error of mean. On the x-axis the three different conditions, pLKO and *RANBP2*^{KD} cells (both shRNAs #1 and #3). The graphs show averages of three independent experiments with at least 40 cells scored per condition. See also supplemental experimental procedures. In WiDr cells (D), the weak category dropped from 71% in controls to 33% with shRNA #1 (p-value=0.02; FDR=0.3) and to 56% with shRNA #3 (p-value= 0.3; FDR=0.7). The null category increased from 18% in the pLKO condition to 62% with hairpin #1 (p-value= 0.003; FDR=0.09) and to 38% with hairpin #3 (p-value= 0.06; FDR=0.5). In HCT116 cells (F), the null category increased from 17% in the pLKO condition to 52% with hairpin #1 (p-value= 0.04; FDR=0.5) and to 44% with hairpin #3 (p-value= 0.01; FDR=0.5).

Figure S4 Sensitivity to vinblastine in a panel of CC cell lines. Vinorelbine Sensitivity in BRAF-like CC Cell Lines is Independent From Proliferation Rate and Similar to Lung and Breast Cancer Cells, Related to Figure 4A, B, C, D, E, F, G, H

(A) WT2 CC cells, *KRAS* mutant non-*BRAF*-like CC cells, (B) *BRAF(V600E)* CC cells and *KRAS* mutant *BRAF*-like CC cells were seeded at low confluence and treated with increasing concentrations of vinblastine twice a week. Viability was assessed by colony formation assay. Cells were fixed, stained and photographed after 10 days of culture.

(C) Sensitivity to vinorelbine is not dictated by differences in doubling time between non-*BRAF*-like and *BRAF*-like CC cells.
The bar graph shows the mean of doubling time (hours) as obtained by IncuCyte of non-*BRAF*-like (LIM1215, Difi, Caco2, HCA-7, HDC54, HCT15, SNU1033, LIM1863, SW480) and *BRAF*-like (Vaco432, WiDr, HT29, RKO, KM20, OXCO-1, SNU-C5, SW1417, HCT116, LoVo, SKCO-1) CC cells cultured for 10 days. Plate density was measured every four hours and related to the average signal on the first day. Data are represented as mean ± standard error of mean (SEM). The p-value (p=0.5) was calculated by using the Mann-Whitney test. See also supplemental experimental procedures.
(D) Boxplot of $\log_{10}$ IC50 values for treatment of *BRAF(V600E)* CC cell lines, WT2 CC cell lines, lung cancer (NSCLC) cell lines and breast cancer (BC) cell lines with vinorelbine extracted from the "Genomics of Drug Sensitivity in Cancer" project. Shown are Log_{10} of IC50 values (µM)
(E) Western blots analysis showing the level of cyclinB1 and cleaved PARP upon 12, 24, 48 and 72 hours of vinorelbine treatment (10nM) in LIM1215, Caco2, HCT15, Vaco432 WiDr and HCT116 CC cells. GAPDH was used as loading control

Figure S5 TGF-β1 Treatment Abolishes the Enhanced Vinorelbine Sensitivity of BRAF-Like RKO Cells, Related to Figure 5C.
(A) Apoptosis induction in RKO CC cells upon RANBP2 knockdown. The level of knockdown of RANBP2 protein and apoptosis induction was measured by western blot
(B-D) TGF-β1 treatment abolishes the enhanced vinorelbine sensitivity of *BRAF*-like RKO cells.
RKO cells were first exposed to recombinant human TGF-β1 for 4 (B), 7 (C) or 10 (D) days and then evaluated in a short term viability assay in presence of vinorelbine (green lines). RKO parental cells exposed to vinorelbine were carried along as control (blue lines). Graphs report the relative survival in the presence of drugs as normalized to the untreated controls after background substraction (See supplemental experimental procedures). Graphs represent the average of three independent experiments. Y-axis indicates the percentage of alive cells. X-axis indicates the serial dilution of vinorelbine (from 100nM to 0.0001nM). Error bars indicate the SD of the three independent experiments.
(E) Western blot experiment showing the extent of activation of TGF-β signaling as measured by phospho-SMAD2 levels at 4, 7 or 10 days of TGF-β1 treatment in RKO CC cell line**.**

Figure S6, related to Figure 6A, B and C.
(A) Intravital imaging of Caco2 (non-*BRAF*-like) and Snu-c5 (*BRAF*-like) CC liver implantation before, 24 hours and 48 hours after treatment with PBS (vehicle). Red dashed lines highlight cells undergoing mitosis. White dashed lines indicate cell fragments. Scale bar, 50 µm.
(B)–(C): related to table S5. In vivo evaluation of DM4 sensitivity in CRC PDX models.
As example of sensitive and resistant response for the in vivo evaluation of DM4 sensitivity in CRC PDX models, CR-LRB-0018P (sensitive model) (B) and CR-IGR-0007P (insensitive model) (C) were grown as tumor derived xenografts in SCID mice. After tumor establishment (150-250 mm^3), mice were treated with ADC-DM4 (40 mg/kg i.v.) or left untreated (control) on the day indicated by an arrow on each graph. Median tumor volumes +/- Median Absolute Deviation (MAD) (n=6 mice per group).

Table S1 Overexpressed genes in BRAF (V600E) colon tumors as compared to BRAF and KRAS wild type (WT2) tumors, Related to Figure 1A, left panel.

Abbreviations: logFC: log fold change; AveExpr: average expression; t: value of the "moderated" t-statistics implemented in limma package for the R statistical software; adj.P.Value: adjusted p-value; pvalue Bonferroni: p-adjusted; diff_log2scale: differential in log2 scale

Table S2 Read Counts for Each shRNA in Each Replicate of shRNA Screen, Related to Figure 1A right panel.

Abbreviations: M: BRAF(V600E); T0: time 0 days; Rep1: Replicate 1; Rep2: replicate2; T13: time 13 days; M_foldChange: BRAF(V600E) fold change; M_padj: p-adjusted for BRAFV(600E); W: WT2; W_foldChange: WT2 fold change; W_padj: p-adjusted for WT2; WM_fold change: WT2/BRAF(V600) fold change

Table S3 Top list of the selected genes from the shRNA screen, Related to Figure 1A, right panel.
Abbreviations: M: BRAF(V600E); T0: time 0 days; Rep1: Replicate 1; Rep2: replicate2; T13: time 13 days; M_foldChange: BRAF(V600E) fold change; M_padj: p-adjusted for BRAFV(600E); W: WT2; W_foldChange: WT2 fold change; W_padj: p-adjusted for WT2; WM_fold change: WT2/BRAF(V600) fold change

Table S4 vinorelbine, vinblastine, paclitaxel IC50 values: 72 hours treatment, Related to Figure 4B.

Each sheet contains the raw data of the IC50 values for the corresponding compounds: vinorelbine, vinblastine, paclitaxel. Values are reported in nM concentration. Cells are categorized as non BRAF-like (in red) and BRAF-like (in green)

Table S5 In vivo evaluation of DM4 sensitivity and BRAF status in CRC PDX models, Related to Figure 6C. Interpretation of the ΔT/ΔC: >40%: inactive (-); ≤40%: marginally active (-/+); ≤ 25%: active with obvious tumor growth delay (+); <10%: tumor stasis (++); <0%: Tumor regression (+++). See extended experimental procedures. BRAF(V600E) mutation in resistant 0/11(0%); BRAF(V600E) mutation in sensitive 4/9 (44%), Fisher 's exact test * 0.026